

We are IntechOpen, the world's leading publisher of Open Access books Built by scientists, for scientists

6,900

Open access books available

186,000

International authors and editors

200M

Downloads

Our authors are among the

154

Countries delivered to

TOP 1%

most cited scientists

12.2%

Contributors from top 500 universities



WEB OF SCIENCE™

Selection of our books indexed in the Book Citation Index
in Web of Science™ Core Collection (BKCI)

Interested in publishing with us?
Contact book.department@intechopen.com

Numbers displayed above are based on latest data collected.
For more information visit www.intechopen.com



Neutron-Stimulated Gamma Ray Analysis of Soil

Aleksandr Kavetskiy, Galina Yakubova,
Stephen A. Prior and Henry Allen Torbert

Additional information is available at the end of the chapter

<http://dx.doi.org/10.5772/68014>

Abstract

This chapter describes technical aspects of neutron-stimulated gamma ray analysis of soil carbon. The introduction covers general principles, different modifications of neutron-gamma analysis, measurement system configuration, and advantages of this method for soil carbon analysis. Problems with neutron-gamma technology in soil carbon analysis and methods of investigations including Monte-Carlo simulation of neutron interaction with soil elements are discussed further. Based on the investigation results, a method of extracting the “soil carbon net peak” from the raw acquired data was developed. The direct proportional dependency between the carbon net peak area and average carbon weight percent in the upper 10 cm soil layer for any carbon depth profile was shown. Calibration of the measurement system using sand-carbon pits and field measurements of soil carbon are described. Measurement results compared to chemical analysis (dry combustion) data demonstrated good agreement between the two methods. Thus, neutron-stimulated gamma ray analysis can be used for *in situ* determination of near-surface soil carbon content and is applicable for precision geospatial mapping of soil carbon.

Keywords: soil carbon analysis, neutron-stimulated gamma ray analysis, Monte-Carlo simulation, Geant4, soil carbon mapping

1. Introduction

1.1. System evolution and application

Neutron-gamma analysis is based on detection of gamma lines that appear due to neutron-nuclei interactions. Many nuclei can be detected and quantified by the presence of these characteristic gamma lines. State-of-the-art nuclear physics methodologies and instrumentation, combined with commercial availability of portable pulse neutron generators, high-efficiency gamma detectors, reliable electronics, and measurement and data processing software, have currently

made the application of neutron-gamma analysis possible for routine measurements in various fields of study. For these reasons, material analysis using characteristic gamma rays induced by neutrons is more wide-spread today; e.g., threat material detection (explosives, drugs, and dangerous chemicals [1]), diamond detection [2], planetary science applications for obtaining bulk elemental composition information, soil elemental (isotopic) content and density distribution [3], archaeological site surveying and provenance studies [4, 5], elemental composition of human [6, 7] and animal [8, 9] bodies, real-time elemental analysis of bulk coal on conveyor belts [10, 11], chloride content of reinforced concrete [12, 13], and in oil well logging [14].

In addition to the aforementioned applications, neutron-stimulated gamma ray analysis can be used in soil science for *in situ* measurements of soil carbon. This method is based on detecting 4.44-MeV gamma rays issued from carbon nuclei excited by fast neutrons promptly after the interaction [15]. Accurate quantification of soil carbon is important since it is an indicator of soil quality [16] that can affect soil carbon sequestration, fertility, erosion, and greenhouse gas fluxes [17–20].

Use of this method for soil elemental analysis has additional advantages over traditional laboratory chemical methods. This is a nondestructive *in situ* method of analysis that requires no sample preparation and can perform multielemental analyses of large soil volumes that are negligibly impacted by local sharp changes in elemental content. These advantages support the use of the neutron-gamma method in soil science.

1.2. General principles of neutron-gamma analysis

Neutron-gamma analysis is based on nuclei issuing gamma rays upon interaction with neutrons (**Figure 1**). Gamma rays are issued due to different processes of neutron-nuclei interactions. First of all, there are inelastic neutron scattering (INS) and thermal neutron capture (TNC) where gamma rays are issued promptly after interaction. New radioactive isotopes can appear due to INS and TNC processes, and decay of these isotopes is accompanied by delay activation (DA) gamma rays.

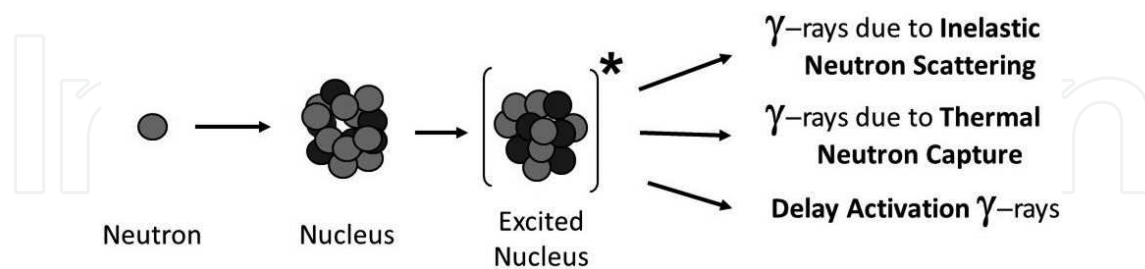


Figure 1. Main processes of neutron interaction with nuclei.

Each kind of nucleus and process produces gamma-rays of particular energy. In some cases, this characteristic gamma line of particular energy can serve as an analytical line for elemental determination. For some elements, the energy of characteristic gamma lines of nuclei and the processes responsible for the appearance of these gamma lines are listed in **Table 1**. As can be seen, gamma ray energy lies in the 1–11 MeV range. This is the range (greater than 1.022 MeV) where the effect of pair production as gamma rays interact with matter is significant. This is why

Element/nucleus	Applied for analysis			
	Kind of neutrons	Process	Cross section, b (neutron energy)	Characteristic gamma line, MeV
Silicon/ ²⁸ Si	Fast	INS	0.52 (14 MeV)	1.78
Oxygen/ ¹⁶ O	Fast	INS	0.31 (14 MeV)	6.13
Hydrogen/ ¹ H	Thermal	TNC	0.33 (thermal)	2.22
Carbon/ ¹² C	Fast	INS	0.42 (14 MeV)	4.44
Nitrogen/ ¹⁴ N	Thermal	TNC	0.08 (thermal)	10.82
	Fast	INS	0.39 (14 MeV)	2.31, 4.46, 5.03, 5.10, 7.03

Table 1. Gamma lines used in neutron-gamma analysis of some elements.

the single escape (SE) and double escape (DE) peaks appear in the gamma spectra near the full energy peak [21]. For example, with carbon registration at full energy peak of 4.44 MeV, peak shifts of 0.511 MeV (SE, 3.93 MeV) and 1.022 MeV (DE, 3.42 MeV) can be observed. The cross sections of INS process for 14-MeV neutron interactions with nuclei are demonstrated in **Table 1**. For instance, the value of the ¹²C cross section at neutron energy of 14.1 MeV is ~0.42 barn. The inelastic scattering of fast neutrons on ¹²C nuclei elevates them to the 4.44-MeV excited energy state [22]. Excited state ¹²C* promptly returns to the ground state issuing the 4.44-MeV gamma ray.



Neutrons lose their energy when propagating through the medium. The interaction cross section depends on energy. The dependence of the INS process cross section with energy for ¹²C is demonstrated in **Figure 2**. The intensity or peak area of this gamma line in the spectrum can be associated with the amount of carbon in a given soil volume. Thus, the registration of the gamma spectra from the studied object caused by neutron interaction with its nuclei can be used for elemental analysis of the object.

1.3. Measurement system configuration

The configuration of a measurement system for neutron-gamma analysis should consist of a neutron source, gamma detector, shielding and construction materials, operational electronics, and data acquisition software. Below we briefly consider the main features of these component parts.

1.3.1. Neutron sources

Isotope neutron sources (based on Cf-252, Am-241-Be, Pu-238-Be isotopes) and portable neutron generators can be used in the measurement setup; some commercially available neutron sources are listed in **Table 2**. Although radioisotope sources are widely used in neutron-gamma analysis [23–26], the use of a neutron generator is preferred (from a radiation safety point of view) since no radiation is produced when the generator is turned “off.” Furthermore, the availability of pulse neutron generators has significantly expanded the possibilities of this method [1, 2, 11, 27].

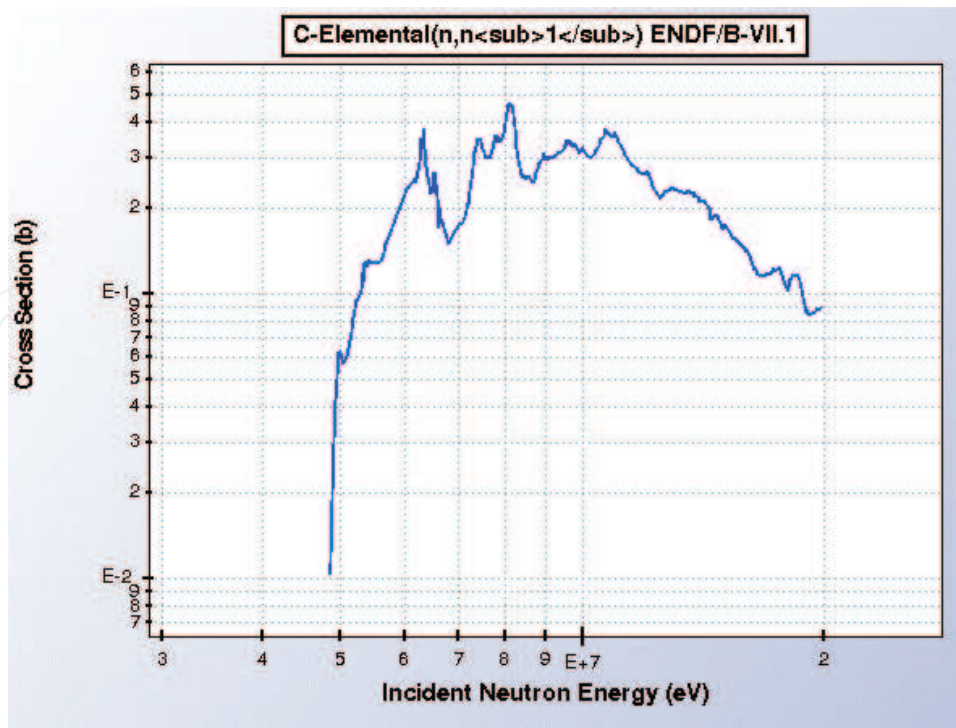


Figure 2. Inelastic neutron scattering cross section of ¹²C nuclei [22].

Type of source	Nuclear reaction	Time of work = T _{1/2} or working mode	Neutron energy, MeV, Avg (max)	Flux, n/s	Reference
Isotope	²⁴¹ Am/Be ²⁴¹ Am → α + ²³⁷ Np α + ⁹ Be → ¹² C + n	432.6 yr	4 (11)	4e7	[22, 28, 29]
	²³⁹ Pu/Be ²³⁹ Pu → α + ²³⁵ U α + ⁹ Be → ¹² C + n	24100 yr	4.5 (10.7)	4e6	[22, 28, 30]
	²¹⁰ Po/Be ²¹⁰ Po → α + ²⁰⁶ Pb α + ⁹ Be → ¹² C + n	138 d	4.2 (10.9)	2.5e6	[22, 28]
	²⁵² Cf spontaneous fission ²⁵² Cf	2.65 yr (alpha decay)	2.3 (6)	4.4e7	[22, 28, 31]
	²²⁶ Ra/Be ²²⁶ Ra → α + ²²² Rn α + ⁹ Be → ¹² C + n	1600 yr	3.9 (13.1)	1.5e7	[22, 28]
Neutron Generator	Genie 16 d + d → n + ³ He	On-Off	2.5	2e8	[32]
	Genie 35 d + d → n + ³ He d + t → n + α	On-Off	2.5	1e8	[32]
			14.1	1e10	
	P 211 d + d → n + ³ He d + t → n + α	On-Off	2.5	1e8	[33]
			14.1		
	P 385 d + d → n + ³ He d + t → n + α	On-Off	2.5	5e8	[33]
			14.1		
	D 711 d + d → n + ³ He d + t → n + α	On-Off	2.5	2e10	[33]
14.1					

Type of source	Nuclear reaction	Time of work = $T_{1/2}$ or working mode	Neutron energy, MeV, Avg (max)	Flux, n/s	Reference
MP320	$d+d \rightarrow n+{}^3\text{He}$	On-Off	2.5	1e8	[33]
	$d+t \rightarrow n+\alpha$ API 120	$d+t \rightarrow n+\alpha$	14.1 On-Off	14.1	2e7
[33] ING	$d+d \rightarrow n+{}^3\text{He}$ $d+t \rightarrow n+\alpha$	On-Off	2.5 14.1	1e8 1e10	[34]

Table 2. Some neutron sources available for use in neutron-gamma analysis.

1.3.2. Gamma detectors

Gamma detectors used in neutron-gamma analysis systems should be suitable for operation in mixed radiation fields where neutrons and gamma rays are present. In ideal cases, detectors should have the following properties [1]:

- detector material must have a high Z value, and total detector volume should be quite large (more than 1 dm³, preferably 5–10 dm³) to effectively detect a relatively low flux of characteristic gamma rays with energy up to ~12 MeV;
- detectors must provide energy resolution that allows for resolving peaks of interest;
- the interaction of neutrons with nuclei in the detector material should not produce gamma rays that overlap useful signals emitted from samples; the detector material should be void of isotopes that are anticipated in analyzed samples;
- neutron activation of isotopes inside the detector volume with time-delayed radiation should be minimal;
- detector sensitivity to changing environmental conditions (temperature, etc.) should be minimal for field application of neutron-gamma analysis.

Satisfaction of these requirements can be difficult, especially due to budget constraints. Among the different types of gamma scintillators, inorganic scintillators are more suitable for neutron-gamma analysis systems due to higher efficiency of registering gamma rays in the energy range up to 12 MeV. The high sensitivity of inorganic scintillation detectors is assured by high gamma ray energy deposition in the relatively large volume (up to several cubic decimeters) of transparent inorganic gamma scintillator mono-crystals with a high Z and density and by their high light yield values (photons per MeV). Semiconductor detectors have a better resolution compared to scintillation detectors, but lower registration efficiency in the desired energy range (up to 12 MeV), which makes scintillation detectors more preferable for use in neutron-gamma analysis systems.

Properties of detectors [based on the sodium iodide NaI(Tl), bismuth germinate BGO, and lanthanum bromide LaBr₃(Ce)] commonly used in the neutron-gamma analysis systems are

described in **Table 3**. Note that other detectors based on inorganic scintillators have worse characteristics and are not usually applied in neutron-gamma analysis.

Detector type	Light yield, photon/MeV	Scintillation decay time, ns	Resolution, % (at 662 keV)	Density, g/cm ³	Effective atomic number*	Reference
NaI(Tl)	38000	250	7	3.67	47	[35]
Bi ₄ Ge ₃ O ₁₂ (BGO)	8200	300	10	7.13	62	[36, 37]
LaBr ₃ (Ce)	70000	17	3	5.07	43	[38, 39]

*Effective atomic number is calculated by [40].

Table 3. Properties of gamma detectors used in neutron-gamma analysis.

1.3.2.1. NaI(Tl)

As shown in **Table 3**, all listed detectors have high light yield. These detectors with sizes around dia 15 × 15 cm provide practically 90% adsorption of gamma rays with energy up to 10 MeV as shown by data in **Figure 3** for sodium iodide detectors. For other detectors, sizes can be less due to higher density and effective atomic numbers. Sodium iodide detectors under neutron irradiation are activated, showing the delayed beta decay spectral continuum with end point energy of 2 MeV [1]. But this activation by neutron fluxes in neutron-gamma analysis does not significantly impact the neutron-stimulated gamma spectra [41]. There are no significant differences in energy resolution before and after irradiation by 4.7×10^{11} of 14-MeV neutrons for the dia 10 × 10 cm NaI(Tl) detector [42]. The radiation damage of sodium iodide occurs at an adsorption dose of 500–1000 Gy [43], which is not accumulated in real time when conducting neutron-gamma analysis.

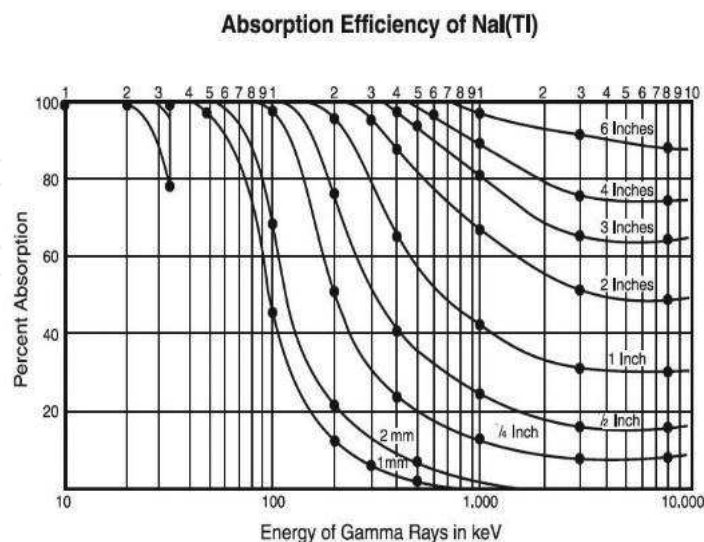


Figure 3. The family of curves derived from NBS circular 583 (1956), Table 37, mass attenuation coefficients for NaI(Tl). Each curve represents the percent absorption (*I*-attenuation) of a parallel beam of gamma rays normally incident on NaI (Tl) crystals of a given thickness [44].

1.3.2.2. BGO

The relatively small light yield of BGO scintillators is compensated by the higher densities and atomic numbers of the composition elements. BGO scintillators have approximately the same efficiency as NaI(Tl), but the interactions of neutrons with BGO elements result in the appearance of gamma lines with energy up to 2.5 MeV, which makes this detector unsuitable for measuring gamma spectra in this range in neutron-gamma analysis [45]. Also, a significant drawback of this type of detector is sensitivity to external temperature [46], but a thermal correction system can compensate for this disadvantage [47].

1.3.2.3. LaBr₃(Ce)

Among inorganic scintillators, LaBr₃(Ce) demonstrated the best resolution and efficiency. Due to the shortest scintillation decay time, this detector had lower background in the high energy part of the spectra due to the smaller number of pile-ups of low energy photons. The presence in this detector of small quantities of the ¹³⁸La radioactive isotope produces a 1.47-MeV gamma peak, which is always visible in the gamma spectrum and can be used for calibration purposes [1], but does not significantly impact the neutron-stimulated spectra. This detector has stable gamma ray spectra parameters when properly shielded against direct neutron flux from the neutron source. It is the best candidate for active neutron applications, but the high cost of this detector (7.62 cm × 7.62 cm LaBr₃(Ce) costs ~US\$35,000 vs US\$2,000 for a high quality NaI(Tl) of similar size [39]) limits a wider use compared to NaI(Tl) and BGO detectors.

1.3.3. Shielding and construction materials

Direct fast neutron flux on the gamma detector and gamma radiation appearing from neutron interaction with detector nuclei leads to high gamma spectra background. High background increases the minimal detection limit of the measurement system and measurement errors. Shielding use between the neutron generator and gamma detector improves characteristics of the measurement system.

Shielding that is one-layer [48–51] or multilayer [52–54] can be used for this purpose. In most cases, fast neutron shielding consists of two or three components which first slows fast neutrons to thermal energy (moderator), absorbs thermal neutrons (absorber), and then attenuates the gamma rays which are produced by different neutrons-nuclei interactions in the moderator and absorber (attenuator). Light materials like water, heavy water, and polyethylene are usually used as neutron moderators, and boric acid is a possible absorber. Sometimes iron is used in the first layer ahead of the light materials to moderate fast neutrons via inelastic neutron scattering [52, 53]. Borated water or borated polyethylene can serve as a combined moderator and absorber in the first layer of shielding. Lead, tungsten, iron, or other such materials with high atomic mass are used to decrease gamma radiation.

While decreasing background, the shielding material and geometry should allow for the counting of useful signal. This means that the shielding thickness should be reasonable and should not produce gamma lines within the energy range of interest. Additionally, it is important to know the possible high energy gamma lines produced from a particular shielding

material since they could interfere with useful gamma lines or give additional continuous background lower energy due to the Compton Effect. Construction materials should have minimal susceptibility to neutron activation by fast or thermal neutrons, issue few gamma rays in the energy range of interest, and have minimum high energy gamma rays that increase system background.

1.3.4. Operational electronics and data acquisition software

Operational electronics and data acquisition software essentially depend on the task and particular method modifications. For example, prompt gamma neutron activation analysis with a radioactive isotope neutron source, a standard gamma detector, and multichannel analyzer (e.g., MCA-1000) with its own software could be used [23]. A complicated custom-made experimental setup consisting of standard Ortec or Canberra electronic blocks paired with a pulsed neutron generator and gamma and alpha detectors can be used for dangerous material detection (as described in [55]). A custom-made electronic scheme and data acquisition software could be used in some cases due to the absence of suitable standard equipment (e.g., NaI(Tl) detector with corresponding electronics and ProSpect v0.1.11-vega software from XIA LLC, Hayward, CA; see Ref. [56]).

1.4. Modifications of neutron-gamma analysis

Depending on the area of application, different modifications of neutron-gamma analysis can be used. Detailed descriptions of these methods were presented in Ref. [27]; we briefly list these methods below:

- PGNAA—Prompt Gamma Neutron Activation Analysis
- PFNA—Pulsed Fast Neutron Analysis
- PFTNA—Pulsed Fast/Thermal Neutron Analysis
- PFNTS—Pulsed Fast Neutron Transmission Spectroscopy
- API—Associated Particle Imaging

Pulsed Fast/Thermal Neutron Analysis (PFTNA) is the most suitable for soil neutron-gamma analysis [57]. The main difficulty conducting soil neutron-gamma analysis is the overlapping of different gamma lines from soil and measurement system nuclei and processes with the main peak of interest (e.g., soil carbon peak). The PFTNA system makes it possible to separate the gamma ray spectrum due to INS reactions ($n, n'\gamma$) from the TNC (n, γ) and DA reaction (e.g., (n, p)) spectra. The moderation and moving neutrons in matter limit the incoming neutron—matter nucleus reaction speed. Approximately 1.5 microseconds are required to moderate 14-MeV neutrons to thermal energy in hydrogenous materials [58], while the lifetime of thermal neutrons can be hundreds of microseconds [59]. Thus, INS reactions will only occur during the microsecond neutron pulse, while TNC processes are running during the neutron pulse and between pulses. One memory address of the data acquisition system records during the neutron pulse, while another memory address acquires data between pulses. This is a technique used with small portable electronic neutron generators (see Table 2). PFTNA employs pulses with a duration of 5–20 microseconds. Microsecond pulse durations

significantly reduce PFTNA system cost compared to pulsed methods using nanosecond neutron pulses. The PFTNA system employs pulse frequencies greater than 5 kHz to ensure nearly constant thermal neutron flux for the measurement period [60]. When operating at 10 kHz and a 25% duty cycle neutron pulse, it was demonstrated that net count rates in the individual peaks of the soil elements silicon and oxygen in the TNC spectrum have a steady state between neutron pulses [61]. Thus, at first approximation, the count rate registration of gamma flux, which appears under neutron irradiation of samples, can be accepted.

2. Neutron-gamma technology for soil carbon determination

2.1. Importance of soil carbon determination

Adoption of agricultural land use practices adapted for climate change and mitigation potential depends on agricultural productivity and profitability. Understanding and evaluating the impacts on soil resources will influence the development of sustainable land use practices. A critical component of any soil resource evaluation process is measuring and mapping natural and anthropogenic variations in soil carbon storage. Soil carbon can impact many environmental processes, such as soil carbon sequestration, fertility, erosion, and greenhouse gas fluxes [17–20]. The current “gold standard” of soil carbon determination is based on the dry combustion technique (DCT) [62]. This method is destructive, time-consuming, and labor-intensive since it involves collecting extensive field soil core samples and requires lots of sample preparation before complex laboratory analysis can be conducted. Furthermore, DCT soil analysis represents a point measurement in space and time that cannot be confidently extrapolated to field or landscape scales which limits its utility for expansive coverage or longer timescale interpretation. Other techniques include laser-induced breakdown spectroscopy, near- and mid-infrared spectroscopy, diffuse reflectance infrared Fourier transform spectroscopy, and pyrolysis molecular beam mass spectrometry [15].

Soil neutron-activation analysis is a new method with the potential for measuring soil carbon in relatively large volumes without having to take destructive soil samples requiring time-consuming standard laboratory analysis. This new method is based on measuring the gamma response of soil irradiated with fast neutrons. One modification of this method, PFTNA—Pulsed Fast/Thermal Neutron Analysis, has been shown to provide wide-area monitoring for prolonged periods [15, 53]. The result of measurements using this method gives, as will be demonstrated below, the values of average carbon content in weight percent in the upper soil layer (thickness ~10 cm) of ~1.5 m² area centered under the neutron source. The measurement time for each surveyed area is 30–60 minutes.

2.2. Problems with neutron-gamma technology in soil carbon analysis and methods of investigation

2.2.1. Features of soil carbon neutron-gamma analysis

The main purpose of this book chapter is to describe the application of neutron-gamma technology for soil elemental analysis. Common features of this technology were described earlier in the introduction. The following aspects of neutron-stimulated gamma ray analysis will be covered:

- mobile neutron-gamma technology systems for soil carbon content determination;
- procedures for measuring the gamma response of neutron-irradiated soil (raw data) and extracting the net soil carbon signal;
- soil carbon depth distribution and the particular soil carbon characteristics that are directly and proportionally dependent on the net carbon signal;
- comparison of neutron-gamma field measurements of soil carbon content to traditional chemical analysis;
- factors impacting gamma response intensity in quantitative soil analysis.

2.2.2. *Methods of investigation*

The methods used for investigating the effects of different factors when applying neutron-gamma technology for soil elemental analysis are:

- Experimental design. Soils being experimentally measured should be around a cubic meter in volume and weigh around a metric ton.
- Deterministic modeling. This method involves solution of integral or differential equations that describe the dependence of behavioral characteristics of the system in question in terms of spatial or time coordinates. This method was used in cases of simple shapes and sample properties (e.g., uniform distribution of elements within the sample volume). This method gives useful semi-quantitative results.
- Monte-Carlo (MC) simulation. The gamma response spectra from modeled soil samples irradiated by neutrons are a very effective method to determine the effect of different factors on the neutron-gamma measurement. An MC simulation model of any sample shape, shielding and detector configuration, or measurement geometry is applicable. MC simulation results are very close to experimental findings.

All these methods were used during our investigations. Results from these methods will be discussed and compared with each other.

2.2.3. *Monte-Carlo simulation method*

MC simulations [63, 64] have been extensively used to solve various problems. For example, MC simulations are capable of estimating the neutron flux passing through materials and their energy loss in these materials, determining the energy distribution of emerging neutrons [65], calculating the optimal thickness of shielding [66, 67] and moderator [68], and reproducing the characteristic neutron-induced gamma-ray spectra of different materials [69–73].

An MC simulation model of soil neutron-gamma analysis should consist of two major components—the measurement system and a soil model. The modeled measurement system should mimic the experimental measurement system. The system could have neutron sources (isotropic source with energies that match the experimental setup), detector, and shielding (if required). The MC simulation soil model can be viewed as a three-phase system (solid, liquid,

and gaseous phases) [74]. Based on calculation objectives, the soil model may be simplified if all soil parameters critical to the MC simulation are met. Our research used the approach of other researchers [74, 75] where the soil model was constructed as a compact medium with known elemental composition and density depth profiles.

The MC simulation describes randomly issued neutron transportation which includes all interactions with soil components until reaching the simulation volume boundary or exhausting its kinetic energy and disappearing due to an interaction. Some neutron-nuclei interactions result in the appearance of gamma rays which move through and interact with soil components. These interactions cause gamma quanta to disappear as they lose energy; however, some will propagate through the soil and be counted by the detector. The simulated gamma spectrum represents the relationship of the gamma count versus energy. The spectrum shape (number of peaks, their intensity) will be influenced by soil properties. The variation of modeled soil properties and MC simulation of the gamma spectra makes it possible to detect the effect of different soil parameters on the shape of the spectra. Note that the MC simulation gave results that were very close to real data.

2.3. Mobile system for soil carbon determination

As previously described [56], our PFTNA system was mounted on a platform that could be transported by tractors or all-terrain vehicles over various field terrains. The dimensions of our mobile platform were 75 cm × 23 cm × 95 cm and weighs ~300 kg. While the primary construction material was aluminum, the iron shielding contributed more weight. Previous findings [53, 76] were used as a basis for the current construction and electronic system requirements. Our PFTNA system had three separate construction blocks (**Figure 4**). Components of the first block were an MP320 pulsed neutron generator (Thermo Fisher Scientific, Colorado Springs, CO), an R2D-410 neutron detector (Bridgeport Instruments, LLC, Austin, TX), and a power system (**Figure 4a, d**). The neutron generator has a pulsed output of 10^7 – 10^8 n s⁻¹ (depending on parameter settings) and neutron energy of 14 MeV. Components of the PFTNA power system were four DC105-12 batteries (12 V, 105 Ah), a DC-AC inverter (CGL 600W-series; Nova Electric, Bergenfield, NJ), and a Quad Pro Charger model PS4 (PRO Charging Systems, LLC, LaVergne, TN). The first block also contained water, iron and boric acid shielding for isolating the detector from the neutron beam and focusing the beam on the soil area of interest. The second block had the gamma ray measuring equipment (**Figure 4b, e**) and contained three 12.7 cm × 12.7 cm × 15.2 cm scintillation NaI(Tl) detectors (Scionix USA, Orlando, FL) with corresponding XIA LLC electronics (XIA LLC, Hayward, CA). For equipment operation, the third block (**Figure 4c**) housed a laptop computer for controlling the neutron generator, detectors, and data acquisition system ProSpect 0.1 (XIA LLC) (**Figure 4c**).

In our applied PFTNA technique, gamma rays emitted by soil chemical elements under pulsed neutron irradiation were divided into two groups: emissions during the neutron pulse due to INS and thermo-neutron capture (TNC) and emissions between neutron pulses due to TNC reaction. Delay gamma rays (i.e., caused by neutron activation reactions) are also captured in these spectra. The two concurrent gamma spectra from each PFTNA measurement (i.e., INS +TNC and TNC spectra) were treated together. Spectra acquisition from the three gamma

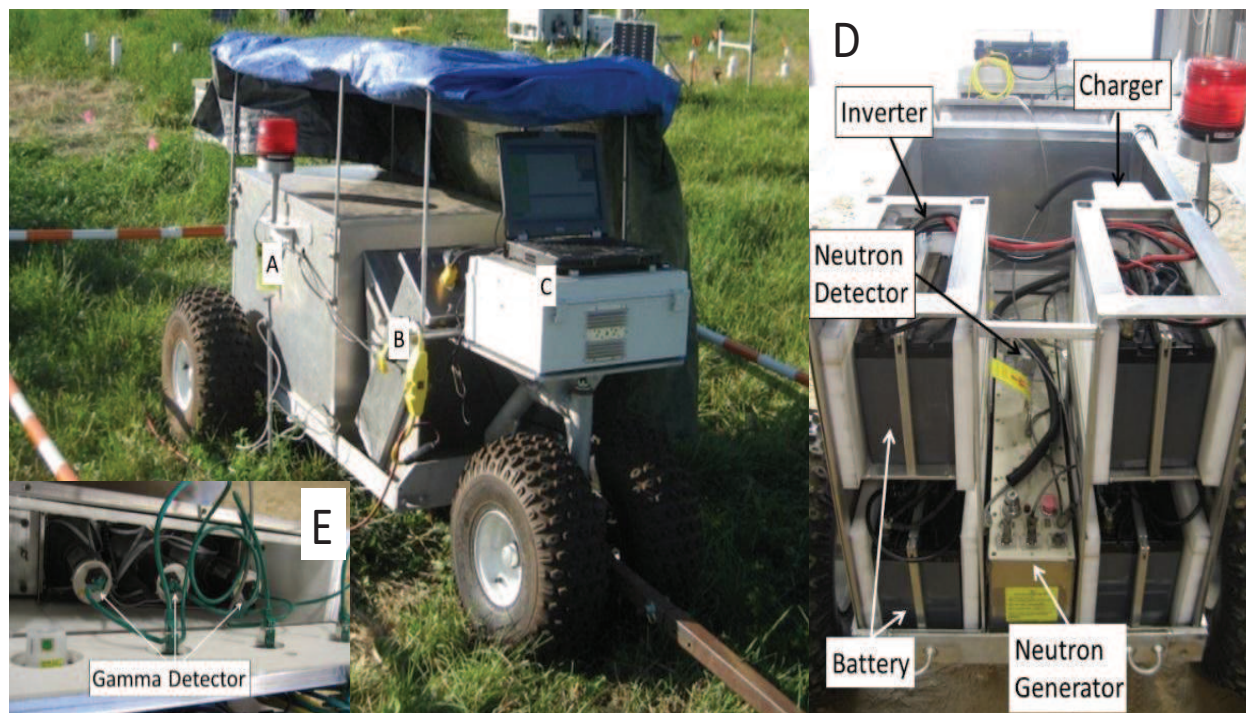


Figure 4. Overview of the PFTNA system: (a) neutron generator, neutron detector, and power system; (b) three NaI (TI) detectors; (c) equipment operation; (d) general view of A showing individual components; and (e) close-up view of the gamma detectors [56].

detectors can be performed in two separate ways. In the first, analog signals from the detectors go to a summing amplifier for processing by a digital multichannel analyzer [77]. In the second, each detector has a dedicated analog-digital converter for spectra acquisition which can be summarized after correction for energy calibration instability [76, 78]. Our testing showed improved resolution from the second method which was therefore adopted for use in our PFTNA. For autonomous operation under field conditions, we developed a mobile power system for reliable equipment operation over extended periods of time. In this mobile PFTNA system, the neutron generator, neutron and gamma detectors, and laptop computer were all powered by four batteries via a power inverter. This inverter transformed 12 VDC battery power to 110 VAC and could operate with input voltages between 10.9 and 14.7 V.

2.4. Raw data acquisition

Two gamma spectra are acquired with our PFTNA measurements: (1) inelastic neutron scattering (INS) spectra acquired during the neutron pulse and (2) thermo-neutron capture (TNC) spectra acquired between neutron pulses. Typical INS and TNC experimental gamma spectra from soil (raw spectra) are shown in **Figure 5** (top and bottom lines, respectively). Each spectrum has a background spectrum and lines due to gamma emission from neutron-irradiated soil elements. The main gamma peak of interest has a centroid at 4.45 MeV in the INS spectrum. This peak may be due to neutron interactions with carbon nuclei and the interference of gamma lines from other nuclei. The oxygen peak (6.13 MeV) and the pair production peak (0.511 MeV) are used as reference points for spectral calibration. The INS spectra consist of gamma rays appearing from inelastic neutron scattering, thermal neutron

capture, and delay activation of nuclei (samples and system construction materials). The TNC spectra consist of gamma rays from all of the above-listed processes except the INS process.

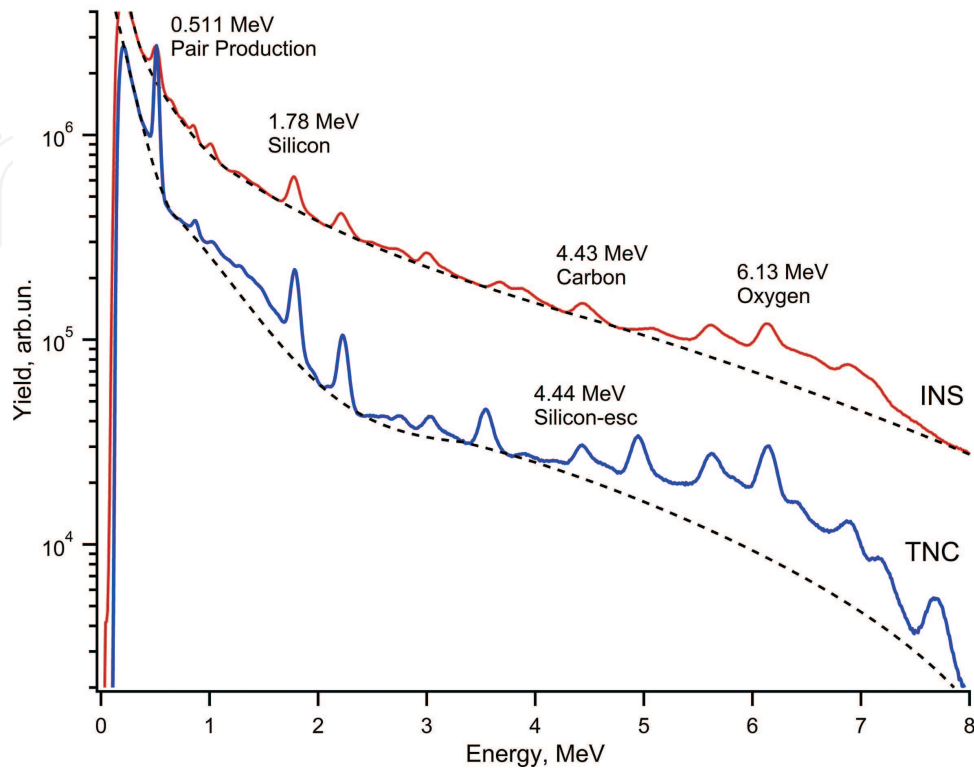


Figure 5. Raw experimental soil gamma spectra [56].

2.5. Extracting the “Net INS Spectra”

The first step in data processing is extracting the “net INS spectra” from raw data. The acquisition time of INS spectra is the duty cycle of neutron pulses multiplied by measurement clock time (minus dead time of multichannel analyzer), while the acquisition time of TNC spectra is one minus the duty cycle of neutron pulses multiplied by time of measurement (minus dead time of multichannel analyzer). Information on acquisition times is made available by the data acquisition software. Thus, spectra can be represented in counts per second (cps). As a first approximation, the number of INS events in some sample volume at some time moment is proportional to the number of fast neutrons in this volume, while the number of TNC events in some sample volume at some time moment is proportional to the number of thermal neutrons in this volume. In the first approximation, the time dependence of the number of fast neutrons $n_f(t)$ can be estimated according to the equation:

$$\frac{dn_f(t)}{dt} = N(t) - \frac{n_f(t)}{\tau_f} \quad (2)$$

where t is a time, $N(t)$ is the neutron flux to the sample from neutron sources, s^{-1} , τ_f is the fast neutron moderation time, s. The fast neutrons convert to thermal neutrons at moderation. The time dependence of the thermal neutron number $n_{th}(t)$ can be estimated as:

$$\frac{dn_{th}(t)}{dt} = \frac{n_f(t)}{\tau_f} - \frac{n_{th}(t)}{\tau_{th}} \quad (3)$$

where τ_{th} is the lifetime of thermal neutrons. As was discussed earlier (see Section 1.4), the fast 14-MeV neutron thermalization time can be accepted as equal to 1.5 microseconds, while the thermal neutron lifetime can be equal to ~ 1000 microseconds. The pulse neutron flux (in neutrons per microsecond) with time can be described by the equation:

$$N(t) = \begin{cases} 40 & \text{if } \text{floor}\left(\frac{t}{200}\right) \leq \frac{t}{200} < \text{floor}\left(\frac{t}{200}\right) + 0.25, \\ 0 & \text{otherwise} \end{cases}, \quad (4)$$

if the neutron flux is 10^7 neutrons per second, frequency is 5000 Hz (pulse time is 200 microseconds), and duty cycle is 0.25 (these pulse neutron generator working regime parameters are for PFTNA of soil).

Solutions for these simple model equations are presented in **Figure 6**. As can be seen, in the frame of this model the time dependence of fast neutron numbers in the sample practically coincides with neutron flux time dependence (**Figure 6a,b**), while the time dependence of the thermal neutron is saw-shaped (**Figure 6c**). If the average value of this “saw” increases at the beginning, the average value reaches a constant value after more than 5000 microseconds (**Figure 6d**). When the “saw” reaches a constant value, the increase in thermal neutrons during the neutron pulse is practically linear with time, and the decrease in thermal neutrons between pulses is also linear (see **Figure 6c**). For this reason, the average value of TNC events and consequently the average TNC gamma flux during the neutron pulses is equal to the average value of TNC events and average TNC gamma flux between the neutron pulses. Hence it is possible to accept that the TNC spectra intensity between pulses is approximately the same as the TNC spectra intensity during pulses (in cps per channel). Based on this consideration, the “net INS spectra” can be restored with channel-by-channel subtraction of the TNC spectra from the INS spectra (both expressed in cps).

2.6. Measurement system background signal

Net INS spectrum represents the gamma rays appearing due to inelastic neutron scattering in both the sample and PFTNA system construction materials. The spectrum due to INS of the system construction materials is the background signal of the measurement system. To measure this background signal, the system has to be spatially removed from large objects (e.g., ground, floor, walls, building ceilings). To achieve this, the PFTNA system could be raised above the ground and away from buildings and large objects by using a crane (**Figure 7**). The measured INS and TNC spectra at different heights above the ground are shown in **Figure 8**; “net-INS spectra” (difference between INS and TNC spectra, both in cps) are shown in **Figure 9**. The peaks in these spectra can be attributed solely to INS processes. Intensities can be evaluated to determine the height at which the signal remained uniform with no change. This “no change” signal is considered to be the net INS system background spectrum.

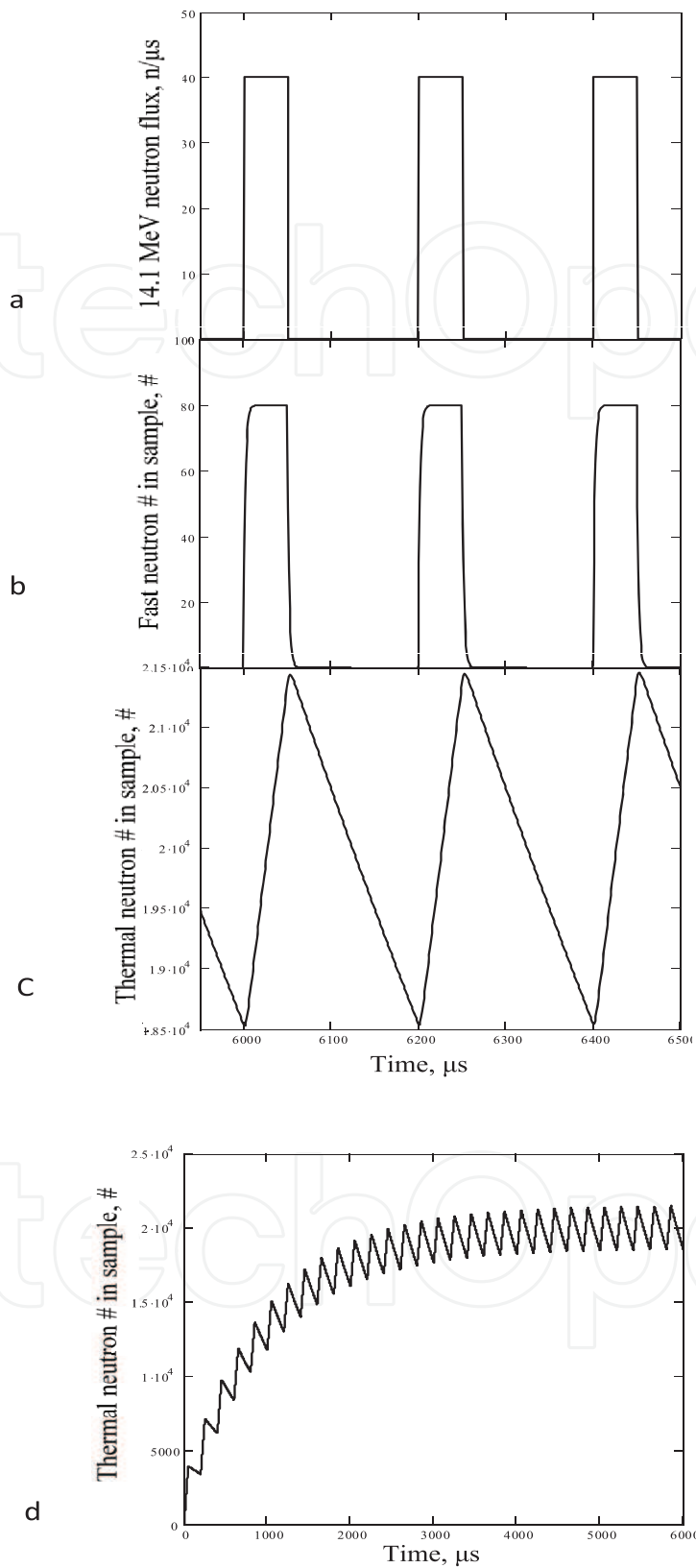


Figure 6. Time dependence of the neutron flux (a), number of fast neutrons in a sample $n_f(t)$ (b), number of thermal neutrons in a sample $n_{th}(t)$ (c), and time dependency of the number of thermal neutron in a sample at a time more less than 6000 microseconds (d).



Figure 7. The PFTNA system background measurements (up to 6.7 m above the ground) [79].

The behavior of peak areas with centroids at 1.78 MeV (“silicon peak,” ^{28}Si), 4.45 MeV (“carbon peak”), and 6.13 MeV (“oxygen peak,” ^{16}O) acquired from the net INS spectra are shown in **Figure 10**. As shown in **Figures 8–10**, some peaks in the spectra decrease and fully disappear with increasing height (e.g., peaks with centroids at 4.95 and 4.44 MeV in the TNC spectra), while other peaks decrease and reach constant values as height increases. Starting at ~4.5 m height, minimal spectral changes are detected. At this height, the measurement system

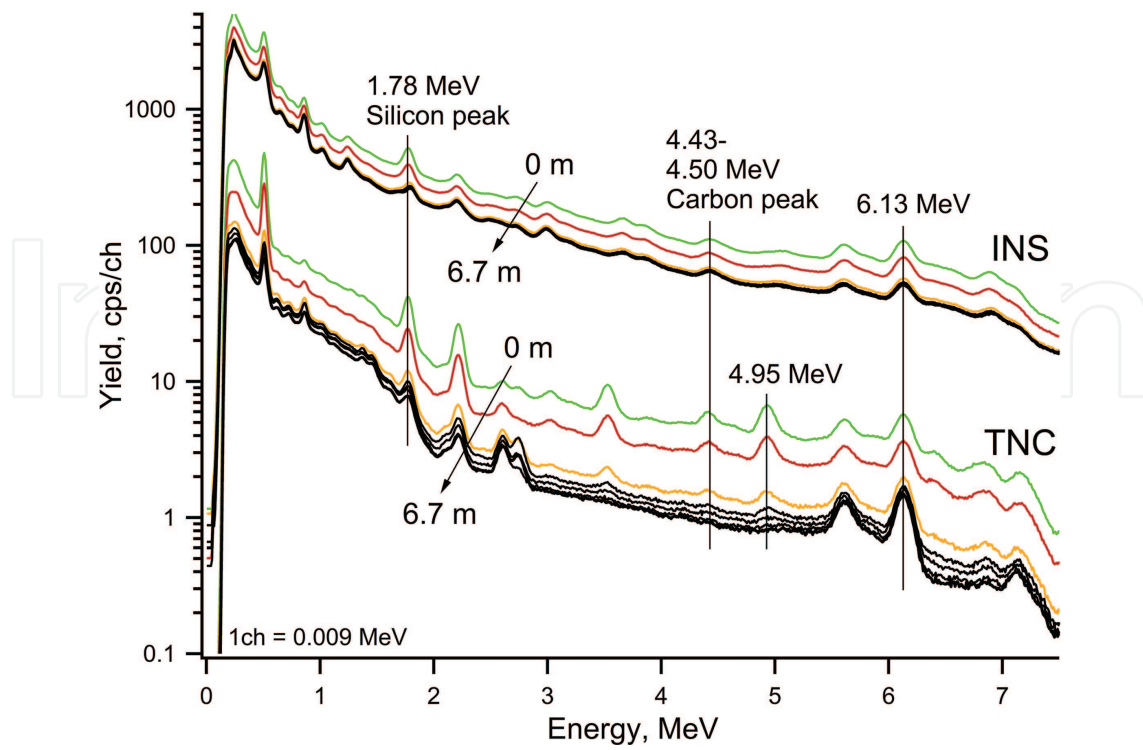


Figure 8. INS and TNC spectra measured by the PFTNA system at different heights above the ground [79].

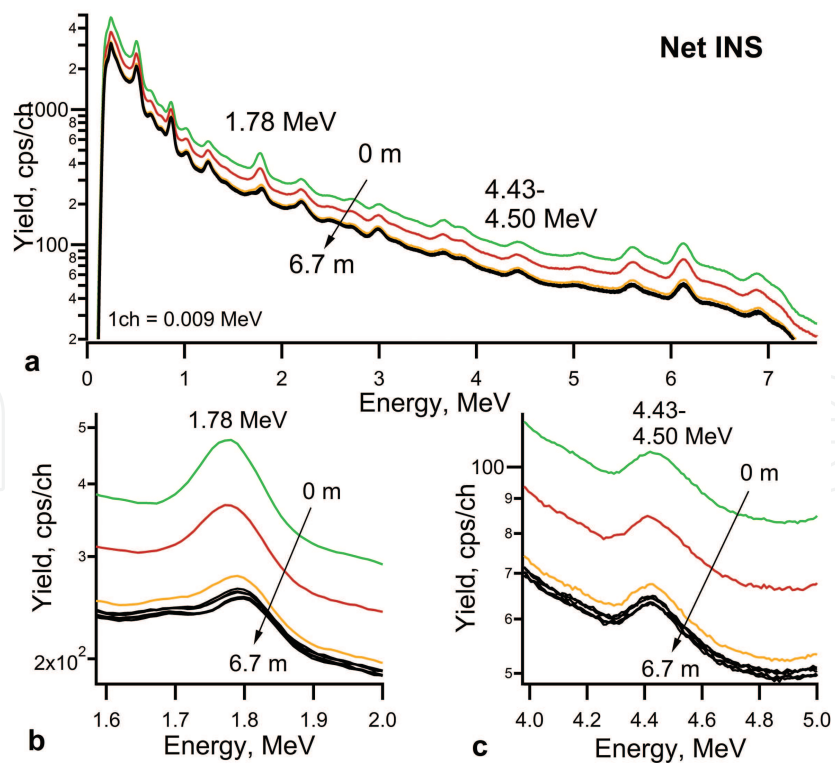


Figure 9. (a) Measurement system net INS spectra (difference between INS and TNC spectra, both in cps) at different heights above the ground; (b) fragment of the net INS spectra around 1.78 MeV; and (c) fragment of the net INS spectra around 4.43 MeV [79].

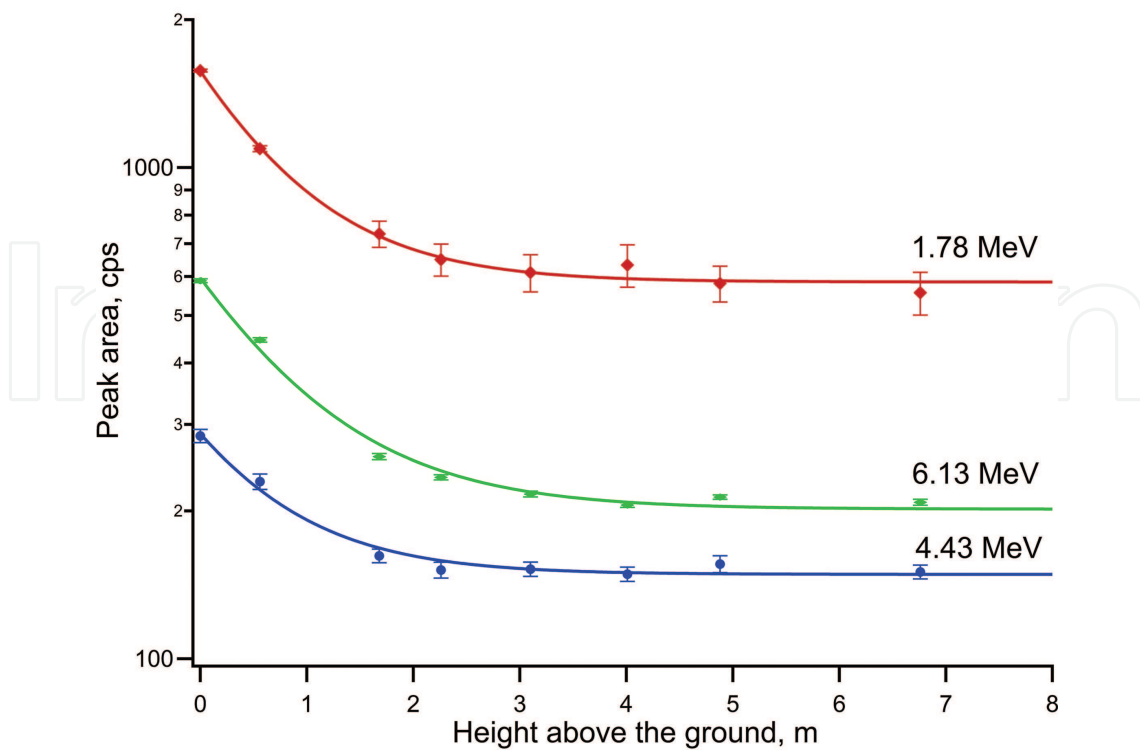


Figure 10. Dependencies of peaks areas with centroids at 1.78, 4.43, and 6.13 MeV in the net INS spectra for measurement system with changing heights above the ground [79].

is far enough away from the ground (and other large objects) that the gamma responses from these objects are negligible compared with the gamma responses from the measurement system construction materials. The net INS spectrum acquired at a height more than 4.5 m could be used as the system background spectrum.

2.7. “Soil Net INS Spectra” and “Soil Carbon Net Peak”

The “soil net INS spectrum” can be obtained from the results of soil measurements and the system background spectra. For this, “the system background net INS spectrum” should be subtracted (channel by channel) from the soil net INS spectrum received from the raw INS and TNC spectra (all spectra should be in cps). The “soil net INS spectrum” consists of gamma rays which appear due to inelastic neutron scattering of fast neutrons on soil nuclei.

Main peak of interest in “the soil net INC-spectra” is the peak with a centroid at 4.45 MeV. Analysis showed (see **Figure 11**) that this peak can consist of the soil carbon peak with centroid at 4.44 MeV, soil silicon cascade transition peak with centroid at 4.50 MeV; possibly the carbon peak with centroid at 4.44 MeV has contribution from excited carbon nuclei as a result of INS on other soil nuclei (e.g., due to $^{16}\text{O} (n, n'\alpha)^{12}\text{C}^* \rightarrow ^{12}\text{C} + \gamma(4.44 \text{ MeV})$ reaction [80]). Silicon ^{28}Si nuclei turn to different excited states due to INS on silicon nuclei. The relaxation of excited silicon passes through the first excited state with energy 1.78 MeV, and the transition to ground state is accompanied by issued gamma rays with energy close to 1.78 MeV (i.e., “soil net silicon peak”). The relaxation of the 6.28 MeV silicon excited state pass to ground state through the first excited state and is accompanied by gamma rays with energy close to 4.50 MeV (6.28 – 1.78 MeV); that is the “silicon cascade transition peak” [22]. This peak can be a part of the 4.45 MeV

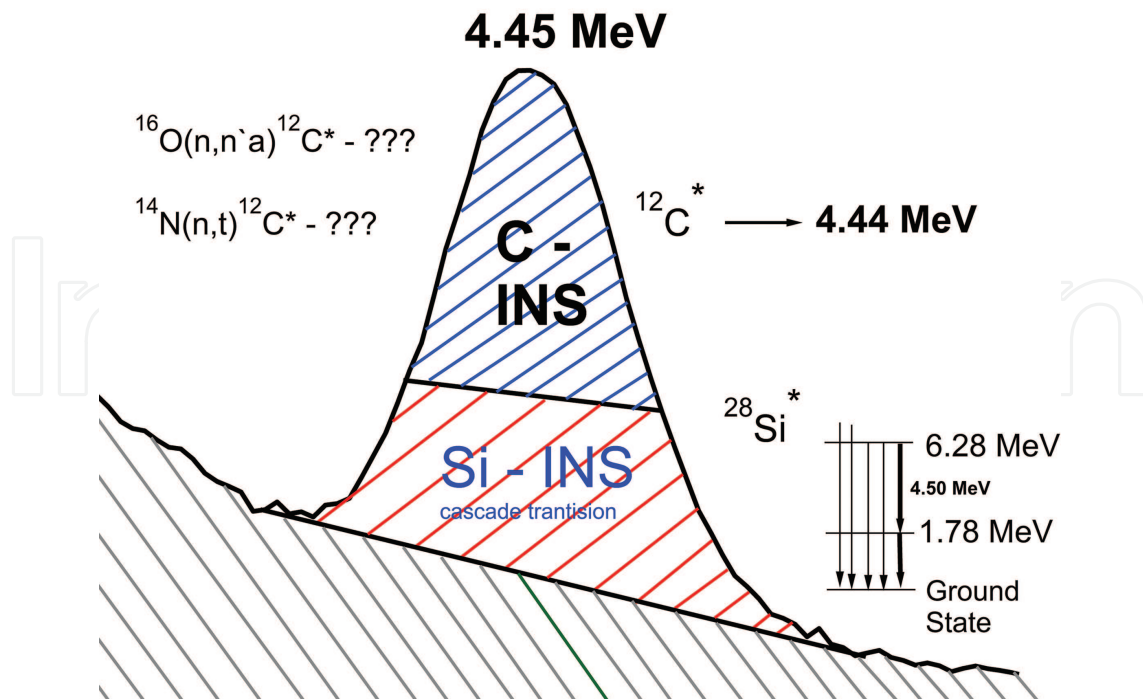


Figure 11. Composition of the 4.45-MeV peak in the soil net INS spectrum.

peak in the “soil net INS spectra.” The theoretical calculation of the 4.50 to 1.78 MeV gamma ray intensity ratio (i.e., “cascade transition coefficient”) gives a value of 0.0547 [81].

2.8. Defining “Soil Carbon Net Peak Area” for a uniform carbon depth profile

2.8.1. Measured gamma spectra of sand-carbon pits

Measurements of INS and TNC spectra using the PFTNA system were performed over 1.5 m × 1.5 m × 0.6 m pits filled with uniform sand-carbon mixtures that had carbon contents of 0, 2.5, 5, and 10 w%. The measurement system was placed over each pit such that the neutron source was situated over the geometric center of each pit. The “soil net INS spectra” were calculated for each pit, taking into account the system background spectra as described above. The experimental “net INS spectra” for pits are shown in **Figures 12** and **13**.

2.8.2. Monte-Carlo simulated gamma spectra of sand-carbon pits

MC simulations of gamma spectra from pits (1.5 m × 1.5 m × 0.6 m) with different sand-carbon mixtures using model geometry very similar to experimental system geometry were evaluated. The soil models are represented as compact media with above-mentioned dimensions and uniform SiO₂+C composition densities

$$d_{mix} = \frac{1.7 \cdot 0.52 \cdot 100}{Cw\% \cdot 1.7 + (100 - Cw\%) \cdot 0.52} \quad (5)$$

where 1.7 is the sand bulk density (g cm⁻³); 0.52 is the coconut shell bulk density used in the pits as carbon (g cm⁻³), and Cw% is the carbon content of the mixture in weight percent. The

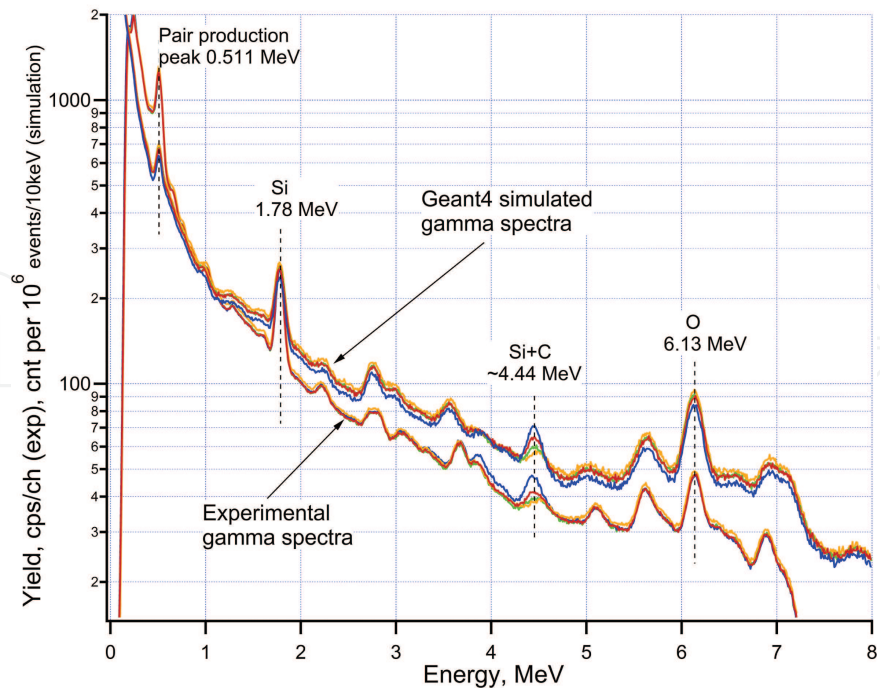


Figure 12. Simulated and measured 14-MeV neutron-stimulated net INS gamma spectra of sand-carbon mixtures (0, 2.5, 5, 10 w% C) in 1.5 m × 1.5 m × 0.6 m pits [79].

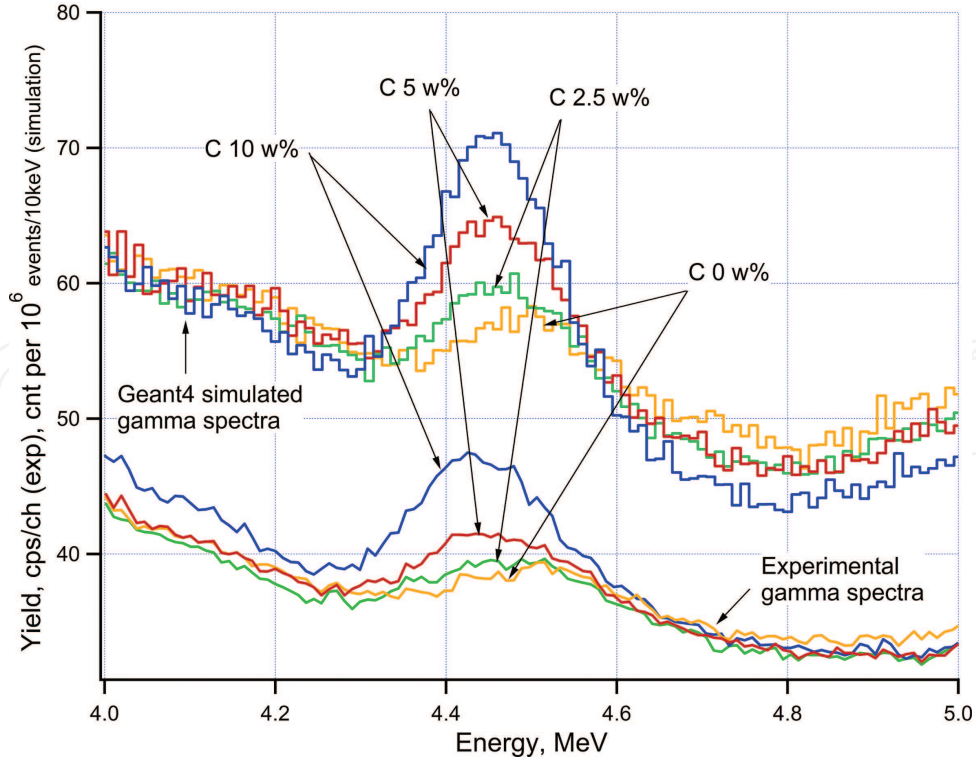


Figure 13. Fragment of simulated and measured 14-MeV neutron-stimulated net INS gamma spectra of sand-carbon mixtures (0, 2.5, 5, 10 w% C) in 1.5 m × 1.5 m × 0.6 m pits [79].

simulation model consisted of a point isotropic neutron source, gamma detector, and shielding similar to the real measurement system. The distance between the source and detector (35 cm), height of the model system above the ground, and number and type of detectors (three NaI(Tl) 12.7 cm × 12.7 cm × 15.3 cm) were the same as in the experimental system. The Geant4 tool kit [82] version G4.10.01p.01 [83] was used to conduct the MC simulations for this and other research issues. A conventional laptop with a multicore processor and high performance computing cluster (Auburn University Samuel Ginn College of Engineering vSMP HPCC consists of 512 cores @ 2.80 GHz X5560, 1.536TB shared memory, and 20.48TB raw internal storage) were used for calculation in the multithread mode. Note that for accuracy of the simulated spectra to approximately equal the experimental accuracy, 10^9 simulation events should be performed. Due to the large number of simulation events, the simulation time for each spectrum was several dozen hours. Our simulation used the neutron cross section JENDL4.0 database rather than the default database (G4NDL4.5) due to the JENDL4.0 simulated spectra and the experimental spectra being more similar. From Geant4 toolkit, we used the QGSP BIC HP and QGSP BERT HP physics lists (Reference Physics Lists, 2014). Both lists had high precision models for neutron transport below 20 MeV and gave the same simulation results. The change in detector energy resolution was taken into account as $\sim 1.142 \cdot \sqrt{E_\gamma}$ (E_γ is the gamma quanta energy, keV) during simulation. This type of energy resolution dependence for gamma detectors is known [84], and the multiplier 1.142 was determined by matching the width of the simulated ^{137}Cs peak to that in the experimental spectra. The detector efficiency dependence with energy was not accounted for since this change would be minor due to the large NaI crystal sizes in the 1–10 MeV energy range [44]. Only INS spectra were simulated; other processes (like thermal neutron capture) in the simulation code were deactivated. A computer screenshot of the simulation model is shown in **Figure 14**.

2.8.3. MC simulated system background “INS spectra”

For determination of “pit net INS spectra,” the system background “INS spectra” should first be simulated. In this simulation, the measurement model geometry and system components (detectors, shielding, sizes) were the same, but the pit model was absent. The “pit net INS spectra” are represented with channel-by-channel differences (simulation channel width is 10 keV) between “pit INS spectra” and system background “INS spectra.”

The effect of system background on the simulated spectra is demonstrated as follows. **Figure 15** represents simulated “INS spectra” of the $\text{SiO}_2+5\text{w}\% \text{C}$ pit measured by a system consisting of a neutron source, sodium iodide detector, and different shielding. The system background spectra with different shielding are also shown in this plot. The “pit net INS spectra” (difference between “pit INS spectra” and “background INS spectra”) are presented in **Figure 16**. As can be seen, the shape of each “pit INS spectra” measured by the system with different shielding is also different. Similar variations were also seen in “background INS spectra” for different shielding, but the “pit net INS spectra” were the same in all cases (**Figure 16**). Although these results may appear trivial, this example demonstrates that parts of system background in the raw spectra can be significant and should be taken into account by subtraction in quantitative analysis. Similar subtractions should be performed in experimental measurements.

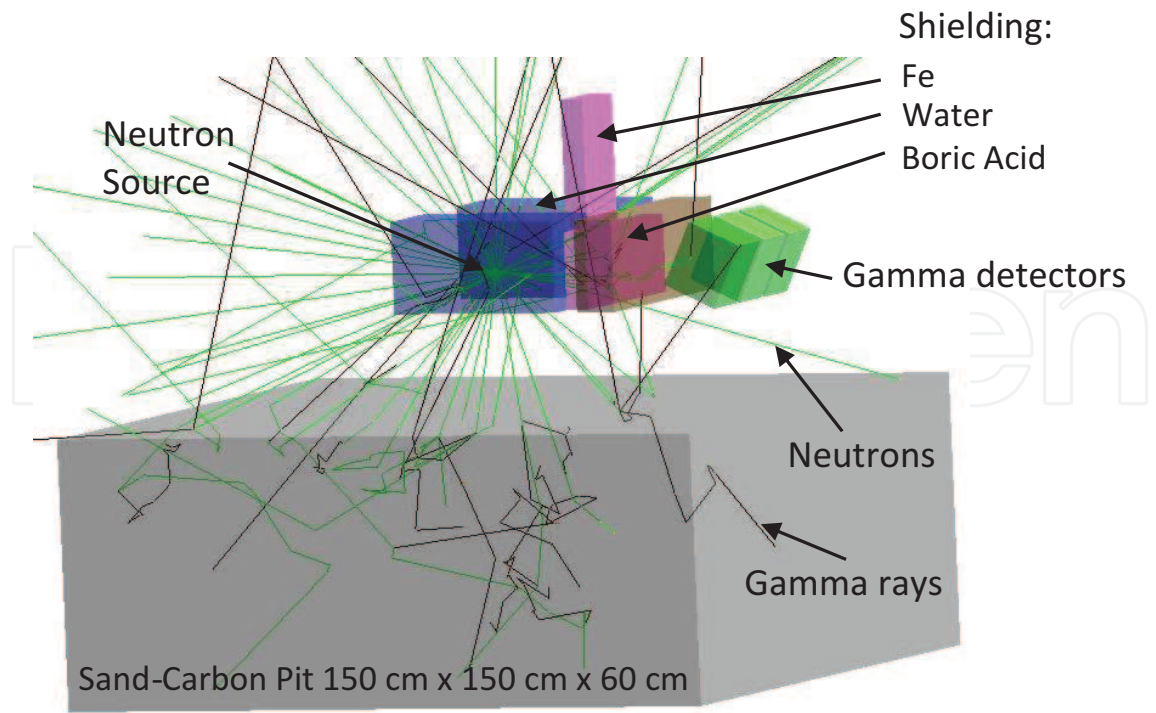


Figure 14. The MC simulation model (Geant4) for measurement of gamma response from a sand-carbon pit under neutron irradiation.

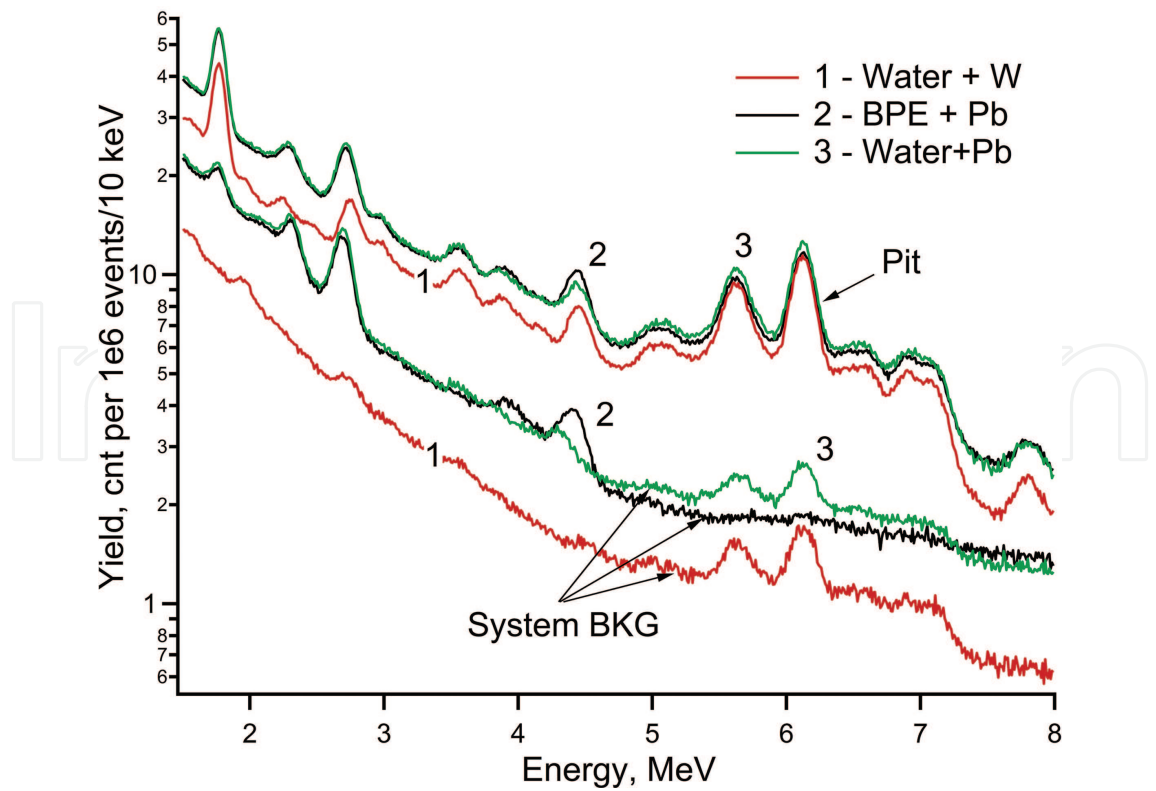


Figure 15. Simulated Geant4 gamma spectra of Pit $\text{SiO}_2 + 5\% \text{C}$ and background for system with different shielding.

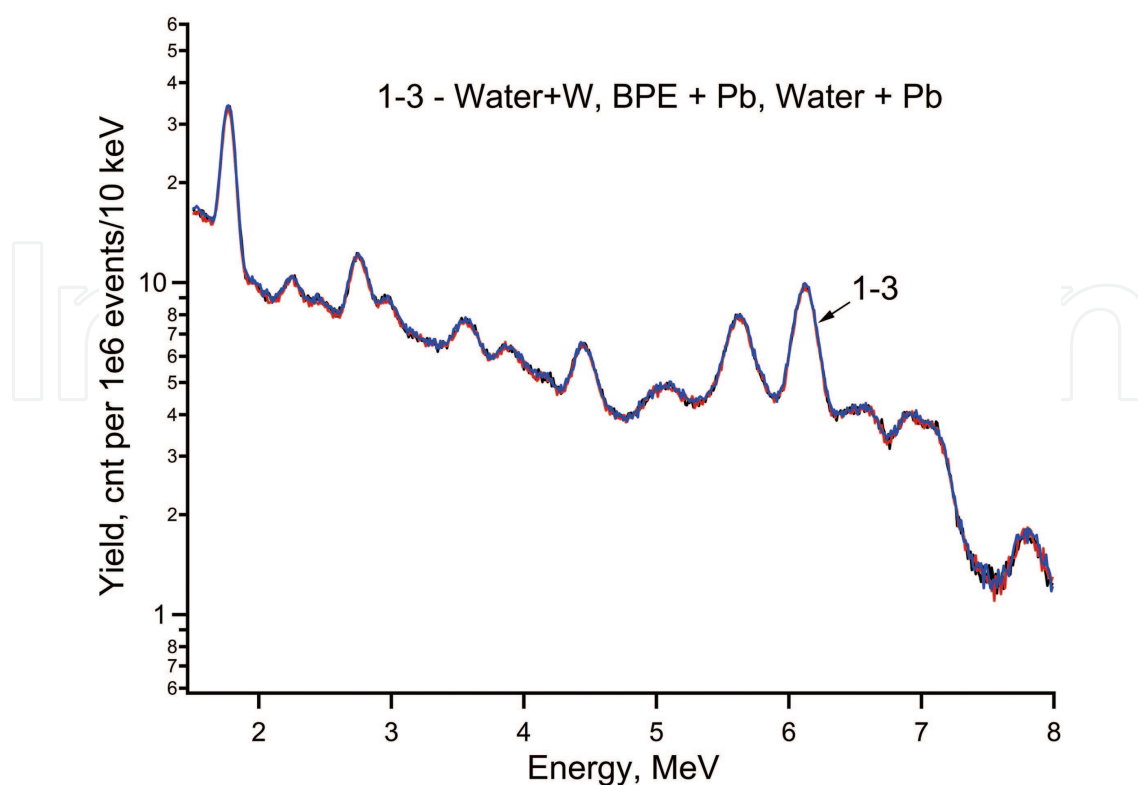


Figure 16. Simulated Geant4 “net pit INS spectra” of Pit SiO₂ + 5%C for system with different shielding.

2.8.4. Dependence of “Soil Carbon Net Peak” area versus pit carbon content

The MC simulated and measured “pit net INS spectra” for pits with different carbon contents are shown in **Figure 12**. As can be seen, the simulated and measured spectra are similar. The simplicity of the model combined with not accounting for the detector efficiency with energy may help explain some differences between measured and simulated spectra. Despite the insignificant discrepancies between measured and simulated spectra, the main features (i.e., position and relative intensity of pair production; and silicon, oxygen, and carbon peaks) are approximately the same, and both were used in our analysis.

Assuming that the “soil carbon net peak” area value can be determined as “4.45 MeV net peak” area minus the “soil silicon net peak” area multiplied by some coefficient f , then the “4.45 MeV net peak” consists of only the “soil carbon net peak” and “silicon cascade transition peak,” with the addition of other gamma rays being negligible. In this case, the dependence of the “soil carbon net peak” area versus carbon content should pass through the “zero-zero” point where the value of this coefficient equals the “cascade transition coefficient.”

To define the dependence of the “soil carbon net peak” area versus carbon content for both the simulated and measured spectra, the “4.45 MeV net peak” area and “soil silicon net peak” area are determined in both the experimental and simulated spectra. In this case, spectral peaks of interest were approximated by one or two Gaussian shape curves using Igor Pro standard software [85] to determine the area beneath the curve. It is important to note that since peak fitting

by summing two Gaussians gives approximately the same value for different component parameters, this sum was used in the analysis rather than the area of the components. An example of the simulated gamma spectra with fitted peaks with a centroid at 1.78 MeV (“soil silicon net peak”) and 4.45 MeV (“4.45 MeV net peak”) by Gaussian shape curves is shown in **Figure 17**.

The “soil carbon net peak area” in the i -th spectrum was denoted as C_{corr_i} . The “soil silicon net peak” area in the i -th spectrum was denoted as SSi_i , “4.45 MeV net peak” area in the i -th spectrum as SC_i , and carbon content in the i -th mixture as $Cont_i$. The assumption was that C_{corr_i} can be calculated as $(SC_i - f \cdot SSi_i)$; C_{corr_i} was considered to be directly proportional to the

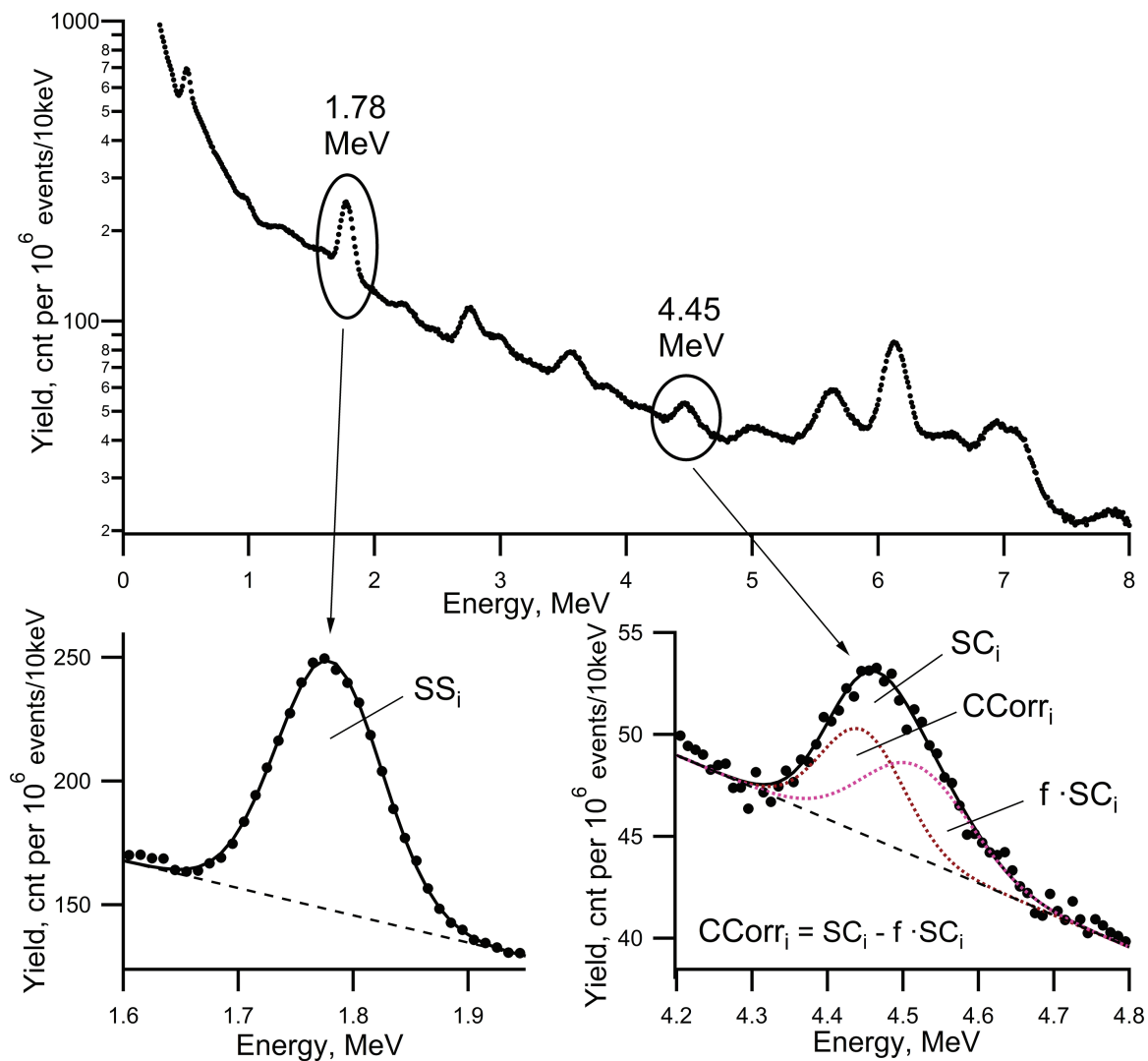


Figure 17. An example of the simulated gamma spectra for the model soil sample and designations of the peak areas used in the calculations: points—simulated data, solid lines—approximation by one (1.78 MeV, “net soil silicon peak”) or sum of two Gaussians (4.45 MeV, “net 4.45 MeV peak”), dotted lines—peak components, and dashed lines—background.

carbon content of the mixture ($k \cdot Cont_i$) with f and k being the coefficients (these designations are shown in **Figure 17** for clarity). Using SC_i and SSi_i data, the values of f and k can be determined by minimizing the expression

$$\sum_i (SC_i - f \cdot SSi_i - k \cdot Cont_i)^2 \rightarrow \min \quad (6)$$

The f and k values were found by equating the derivatives of this sum with respect to f and k set to zero. These calculations were performed using the standard mathematical software, MathCAD (Parametric Technology Corporation, 2013).

The dependencies between the “4.45 MeV net peak” area, “soil silicon net peak” area, and “soil carbon net peak” area C_{corr} with carbon content from simulated and measured spectra are presented in **Figure 18**. As can be seen, the dependencies in both cases are similar to each other and pass through the “zero-zero” point. In addition, the values of the coefficient f from data processing of both the experimental and simulated spectra are very close (0.054 and 0.058, respectively). Values of this parameter (i.e., coefficient of the cascade transition for ^{28}Si nuclei) are similar to earlier published values [81, 86]. Thus, it is possible to define the “soil carbon net peak” area (from the “soil net INS spectra”) as “4.45 MeV net peak” area minus “soil silicon net peak” area multiplied by some coefficient f , where f is the “cascade transition coefficient” equal

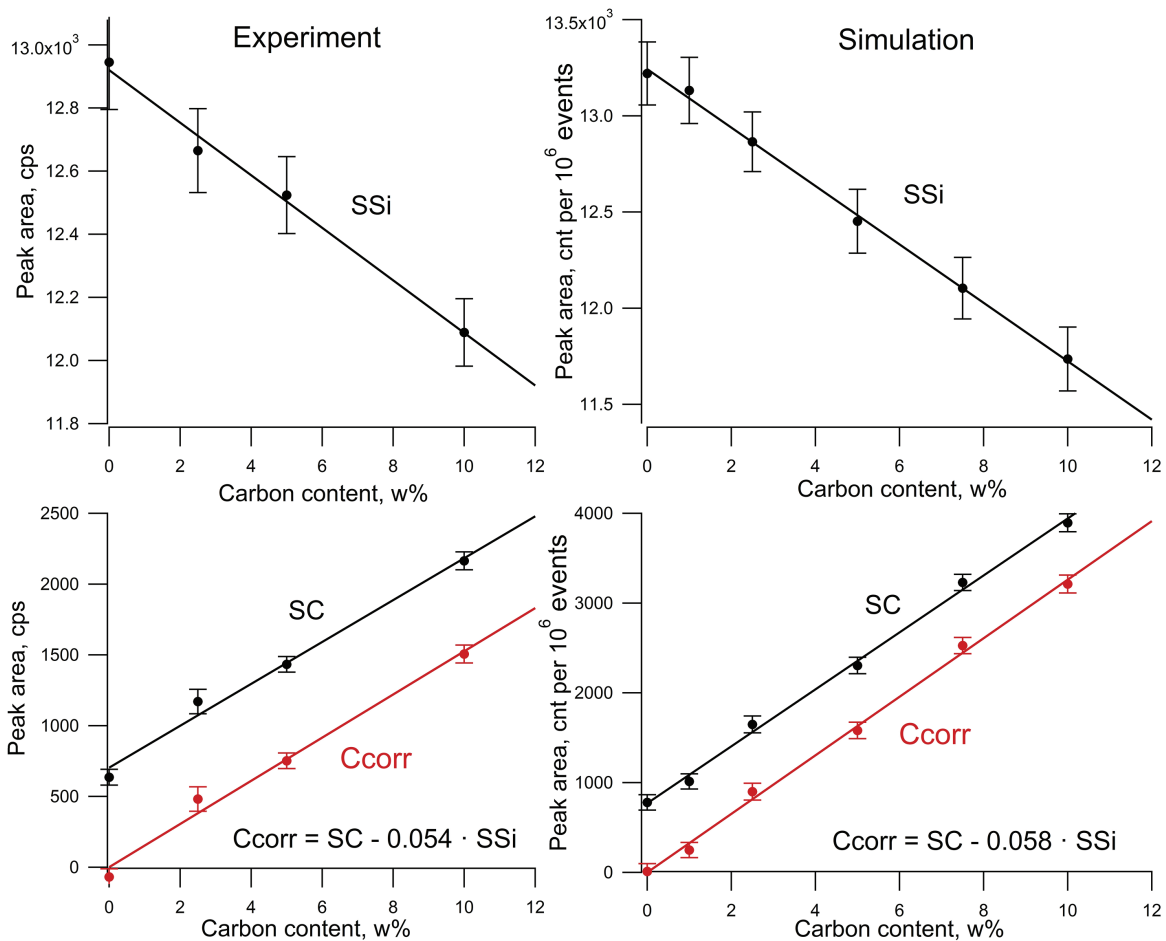


Figure 18. Dependencies of the “4.45 MeV net peak” area SC, “soil silicon net peak” area SSi, and “soil carbon net peak area” C_{corr} with carbon content from the simulated and measured spectra of sand-carbon mixtures [79].

to 0.0547 without taking into account the effect of other INS processes like $^{16}\text{O}(n,n'\alpha)^{12}\text{C}^* \rightarrow ^{12}\text{C} + \gamma$ (4.44 MeV).

2.9. Parameter selection for soil carbon characterization

The carbon gamma signal intensity (“soil carbon net peak” area) measured by the gamma detector is dependent on neutron flux intensity and soil conditions (density and element content), but the gamma signal intensity can be strongly influenced by the distribution of carbon within the soil depth profile. Neutron penetration depth and gamma flux attenuation are determined by soil properties. The distribution of soil carbon with depth is usually nonuniform (i.e., carbon level decreases as depth increases) and by first approximation can be described by exponential law [15]. The parameters of these distributions vary from site to site [56]. For this reason, correlations between the carbon peak intensity in the gamma spectrum and characterization of soil carbon content parameters are not obvious.

2.9.1. Parameter candidates

The main problem is determining which characteristic of soil carbon content has a direct proportional dependency (even in some approximation) with “soil carbon net peak” area. In general, the average carbon content or integral by some depth can be used to characterize the carbon in some depth layer. The tested candidates were average parameter—average carbon weight percent in some soil layer ($AvgCw\%(h)$, where h is the layer thickness) and integral parameter—grams carbon per square centimeter of soil surface in a layer of some thickness ($SD(h)$, surface density). These parameters can be calculated as:

$$AvgCw\%(h) = \frac{1}{h} \int_0^h W\%(b) db \quad (7)$$

$$SD(h) = \int_0^h W\%(b) \cdot d(b) db \quad (8)$$

where $W\%(b)$ is carbon weight percent at depth b and $d(b)$ is the soil density at depth b . Note that another possible characteristic will be proportional to one of these characteristics.

2.9.2. “Surface Density in 30 cm” parameter

Ref. [15] reported that the value of the carbon signal in INS spectra was connected to the surface density of carbon in a 30-cm layer. **Figure 19** shows three carbon depth profiles in modeled sand-carbon mixtures for which the values of $SD(30)$ are all equal to 2.29 gC cm^{-2} . But the fragment of the MC simulated INS spectra around the carbon peak (**Figure 20**) for these modeled sand-carbon mixtures illustrates that these peaks are quite different despite $SD(30)$ being the same for all mixtures. Thus, the “soil carbon net peak” area is not directly proportional to soil carbon content expressed in carbon surface density at 30 cm; this indicates that some other parameter should be found.

The effect of carbon depth profile and soil elemental content on the gamma spectrum as a whole (particularly for the carbon peak) can be determined from experimental results for soil sites with different carbon depth profiles, and by varying the carbon depth profile

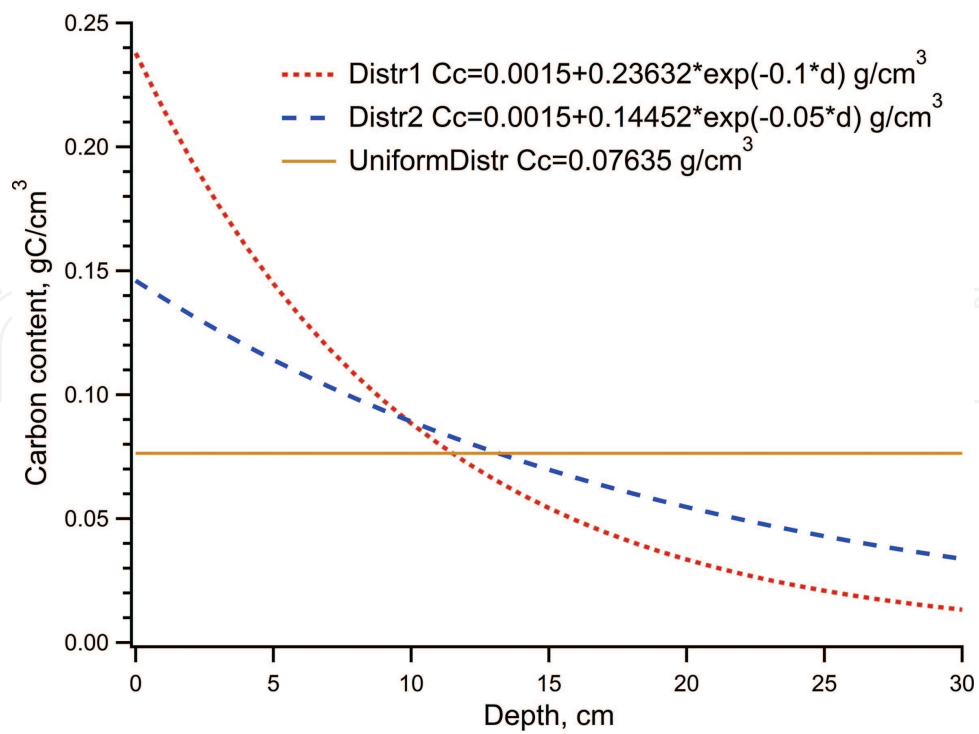


Figure 19. Carbon depth profiles in modeled sand-carbon mixtures for which the value of $SD(30) = 2.29 \text{ gC cm}^{-2}$.

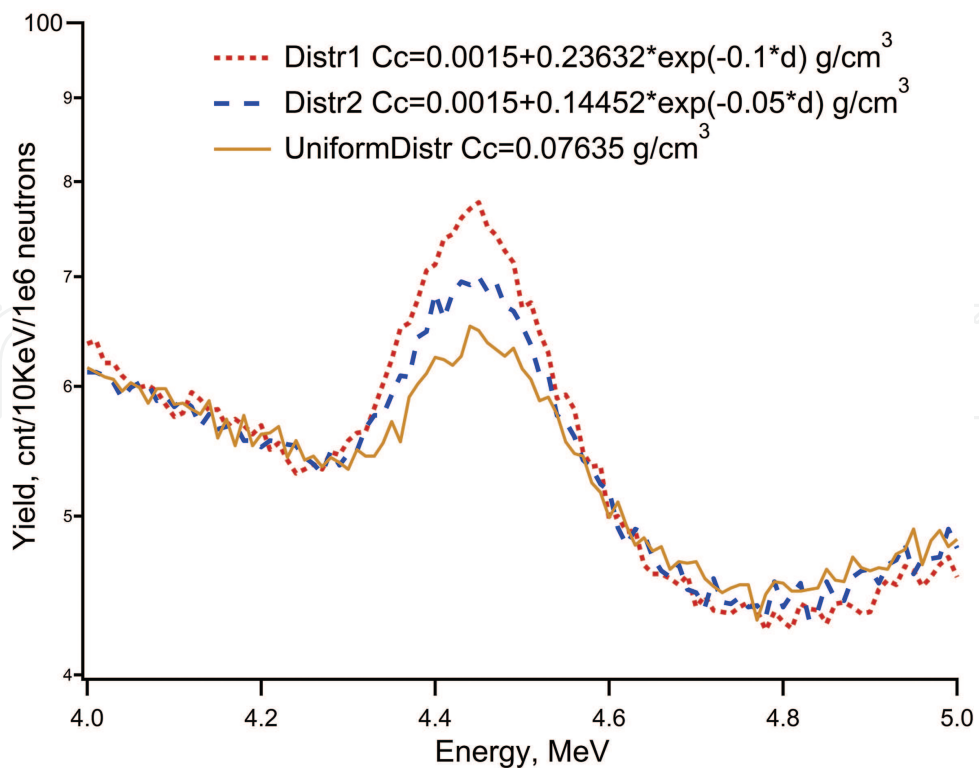


Figure 20. Fragment of MC simulated INS spectra (around the carbon peak) of modeled sand-carbon mixtures with carbon depth profiles shown in Figure 19. For all cases $SD(30) = 2.29 \text{ gC cm}^{-2}$.

parameters in the soil model during MC simulations. These measurements and simulations were done to further our understanding of the relationship between INS signals and soil carbon content.

2.10. “Net INS Spectra” for nonuniform carbon depth profile sites

2.10.1. Carbon, soil density, and main element depth profile examples

Figures 21–23 show carbon depth profiles, soil density examples, and main element depth profiles from sampling sites. These carbon depth profiles were from an applied field (AF) located at the Piedmont Research Unit, Camp Hill, AL, USA [41]. Data was from traditional dry combustion chemical analysis of cores collected from the AF sites. Dependencies shown in Figures 21–23 were used to construct the soil model in the simulation. Six artificial carbon depth profiles with extremal shapes (Art1–Art6 in Figure 21) were also used in the simulations.

2.10.2. Measured and simulated net INS spectra for sites with nonuniform carbon depth profile

Raw INS and TNC spectra were collected for each site and replotted in units of “counts per second.” Afterwards, “soil net INS spectra” were calculated taking into account the “system background spectra” data (as was described above). For MC simulation, “soil net INS spectra” were calculated by subtracting the previously simulated system background spectra from the “soil INS spectra.” Examples of measured and simulated spectra for some of these areas are

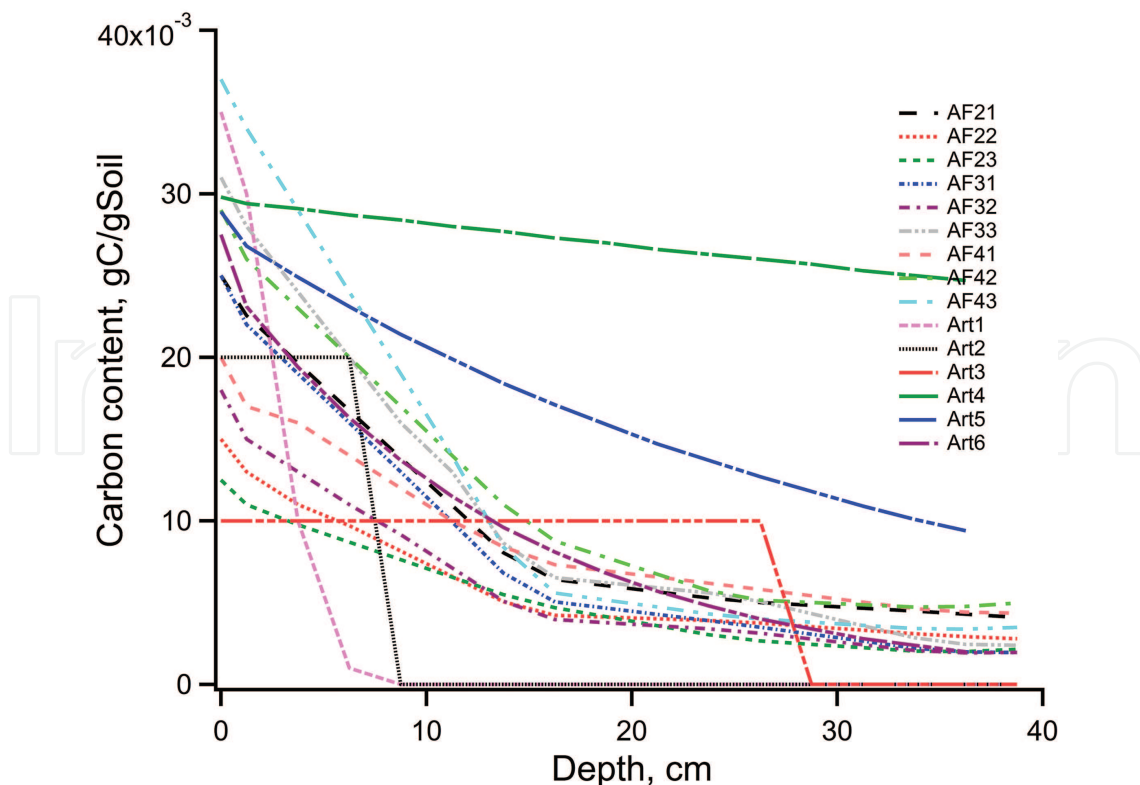


Figure 21. Soil carbon depth profiles for different sites (see text for details) [79].

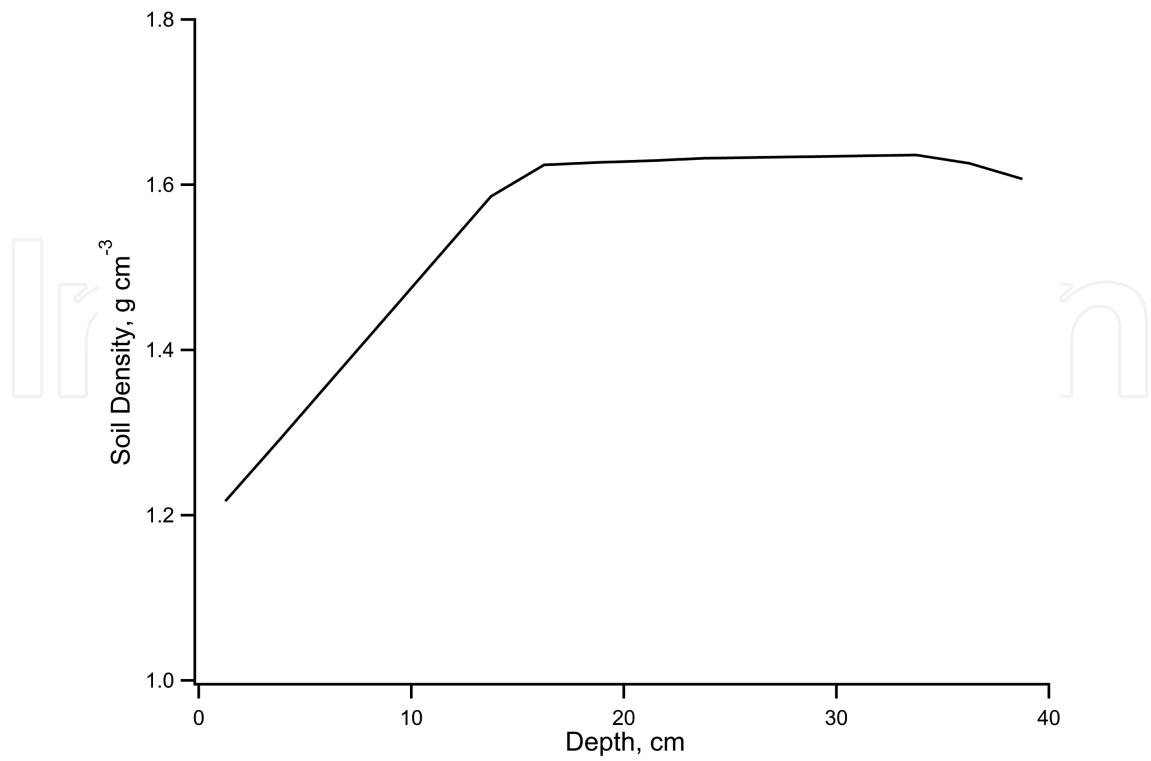


Figure 22. Soil density depth profile for the experimental site [79].

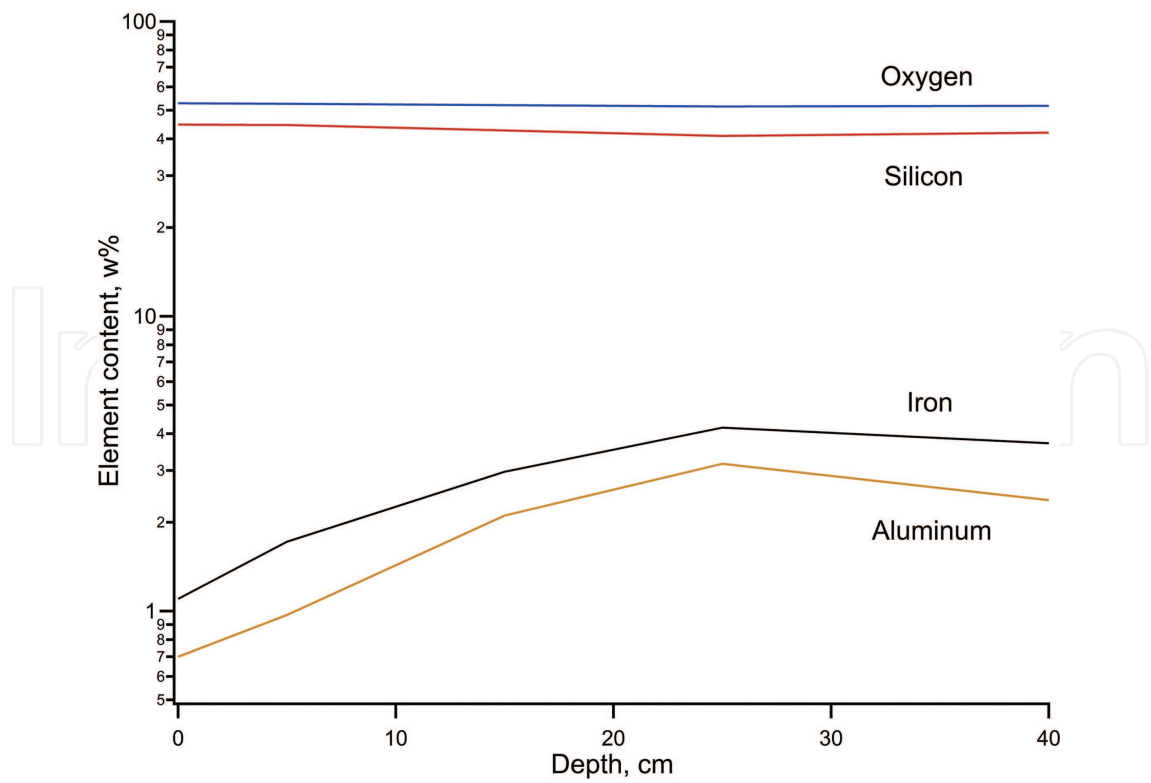


Figure 23. An example depth profile of the main soil elements [79].

shown in **Figure 24**. As can be observed, the simulated and measured spectra were very similar to each other. The peak areas with centroids at 1.78 and 4.45 MeV were calculated from these spectra using approximation by one or two Gaussian shape curves with Igor Pro standard software [85]. Next, “soil carbon net peak” area was defined using the above described procedure by subtracting the “soil silicon net peak” multiplied by the “cascade transition coefficient” (i.e., 0.0547) from the “4.45 MeV net peak” for each measurement and simulation.

2.10.3. Calibration

The calibration coefficient to calculate the carbon content from the value of “soil carbon net peak” area was determined from the gamma spectra for pits with uniform sand-carbon mixtures. Carbon content can be denoted in units of the average carbon weight percent or surface density. For uniform sand-carbon mixtures, the calibration line “soil carbon net peak” area versus $w\%$ will not depend on the thickness, while the calibration line “soil carbon net peak” area versus SD will depend on the given thickness. The carbon characterization parameter should be applied for any carbon depth profile, including uniform distribution. Thus, it should be possible to use the calibration coefficients derived from uniform distribution to calculate the carbon characterization parameter for the spectra of sites with nonuniform carbon depth distribution.

Calibration dependencies for uniform sand-carbon mixtures were also constructed for simulated and experimental spectra. In this case, the coefficients f and $k_{w\%,j}$ and $k_{SD,j}$ ($j = 1$ for measurement, $j = 2$ for MC simulation) were determined as described above by Eqs. (7) and (8) for both cases, where $Cont_i$ corresponded to $W\%$ or $SD(h)$. For uniform mixtures, $AvgCw\%$ does not depend on h . Thus, there is only one set of coefficients f and $k_{w\%,j}$. SD depends on h ; therefore, each h has its own set of coefficients, f and $k_{SD,j}(h)$. In the set of coefficients for SD , the coefficient f is the same for each h and approximately the same for f for weight percent. Using the determined coefficients, the dependencies of the “soil carbon net peak” area (C_{corr}) in the measured and MC simulated spectra versus carbon weight percent and versus carbon surface density at different thicknesses [$SD(h)$] in sand-carbon mixtures samples were plotted (**Figures 25** and **26**). These figures illustrate that the dependencies of C_{corr} with $W\%$ and with $SD(h)$ are directly proportional within measurement and simulation accuracy limits in all cases.

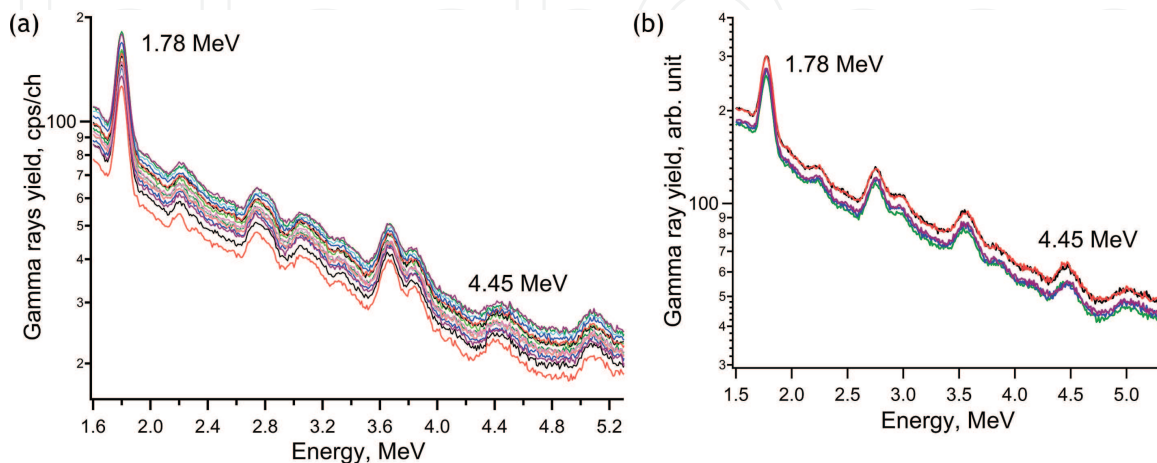


Figure 24. Measured (a) and MC simulated (b) “net soil INS gamma spectra” of different sites with characteristics shown in **Figures 21–23**.

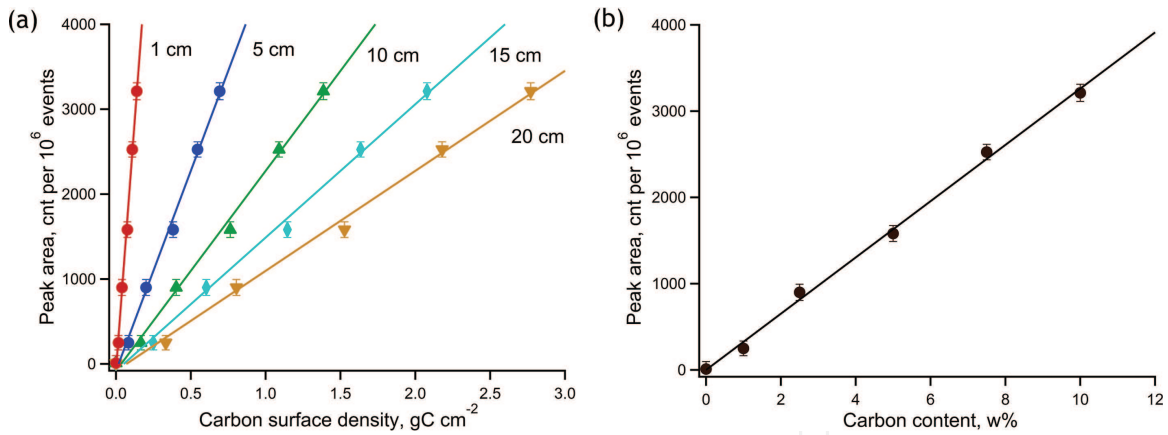


Figure 25. Calibration lines plotted from data of MC simulations [79]: (a) “net soil carbon peak” area versus carbon surface density; thickness shown near line; (b) “net soil carbon peak” area versus carbon weight percent.

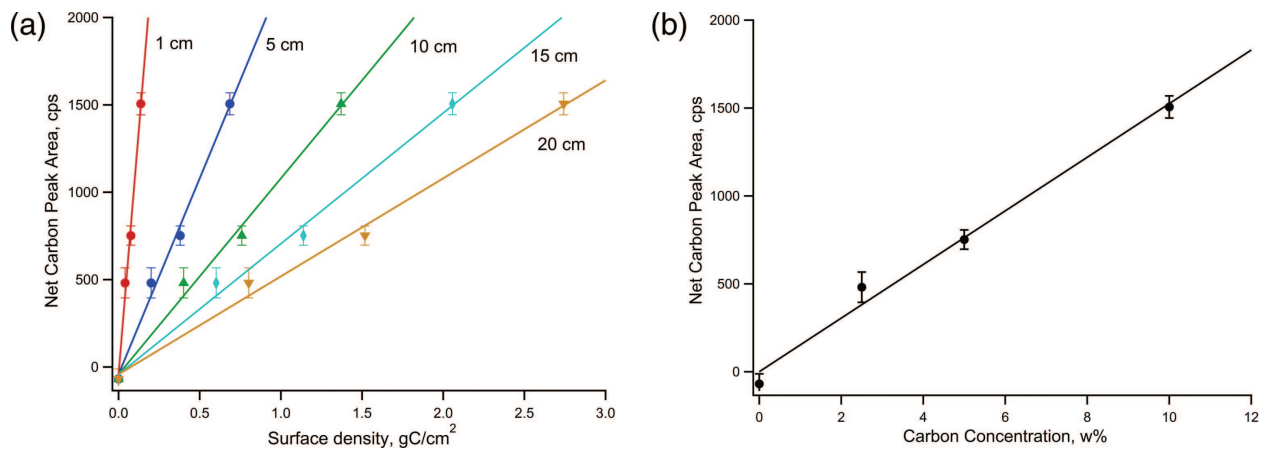


Figure 26. Calibration lines plotted from measurement data: (a) “net soil carbon peak” area versus carbon surface density; thickness shown near line; (b) “net soil carbon peak” area versus carbon weight percent [79].

2.11. Comparison of PFTNA and chemical analysis data

The calculation of $AvgCw\%(h)_{DC,i}$ and $SD(h)_{DC,i}$ by chemical analysis (dry combustion) was done for each site to compare with the data received from the INS gamma spectra. Coincidence of values for some parameters received from the net soil INS gamma spectra and from chemical analysis will mean the value of this parameter can be determined from neutron-gamma measurements.

2.11.1. Dependence of average values of relative differences with h

For each site, the relative difference between $Cw\%_{INS,i,j}$ and $SD_{INS,i,j}(h)$ for INS and MC simulation data and $AvgCw\%(h)_{DC,i}$ and $SD(h)_{DC,i}$ values from soil chemical analysis data were used to compare these values.

$$rw_{\%i,j}(h) = \frac{AvgCw\%(h)_{DC,i} - Cw\%_{INS,i,j}}{Cw\%_{INS,i,j}} \quad (9)$$

$$rSD_{i,j}(h) = \frac{SD(h)_{DC,i} - SD_{INS,i,j}}{SD_{INS,i,j}} \quad (10)$$

The relative difference values for each site with h were calculated and plotted. The example of $rw\%_{i,2}(h)$ for different sites is shown in **Figure 27**. This relative difference was found to be equal to zero at some layer thickness h for each site. As can be seen in **Figure 27**, this depth varies around 10 cm in the range of ± 2 cm for all sites.

The dependence of average values of relative differences for weight percent and for surface densities, $\xi w\%_j(h)$ and $\xi CD_j(h)$ for all surveyed sites with h , were calculated as

$$\xi w\%_j(h) = \frac{1}{N_j} \sum_i \frac{AvgCw\%(h)_{DC,i} - Cw\%_{INS,i,j}}{Cw\%_{INS,i,j}} \quad (11)$$

$$\xi CD_j(h) = \frac{1}{N_j} \sum_i \frac{SD(h)_{DC,i} - SD_{INS,i,j}}{SD_{INS,i,j}} \quad (12)$$

where N_j is the number of the sites used in measurements ($j = 1$) and in MC simulations ($j = 2$); both demonstrated some form of regularity. These dependencies are shown in **Figure 28** for both measurements and MC simulations.

Equality $\xi w\%_j(h)$ or $\xi CD_j(h)$ value to zero means that, at this h , the soil carbon characteristics determined from the spectra and from depth distribution are very similar. As one can see, the carbon weight percent derived from the spectra coincides with the average weight percent at a thickness of ~ 10 cm. **Figure 28** shows that the values of surface density from the spectra and from depth profiles differ from each other at any thickness. From these results we conclude

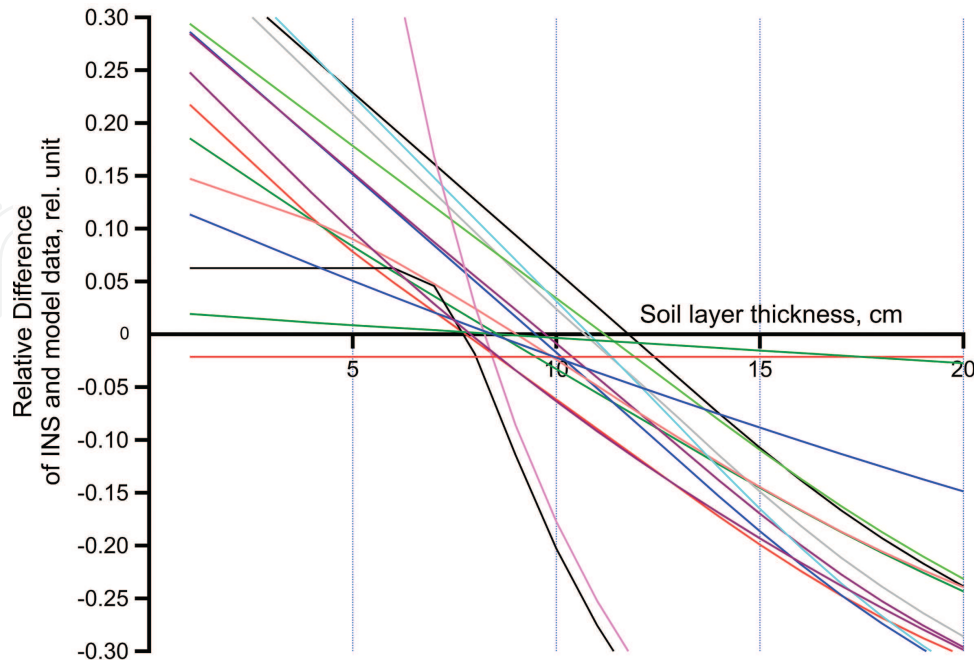


Figure 27. The dependence of the relative difference between $Cw\%_{INS,i,j}$ for data received from MC simulation and $AvgCw\%(h)_{DC,i}$ values from chemical analysis data with h for sites used for MC simulations [79].

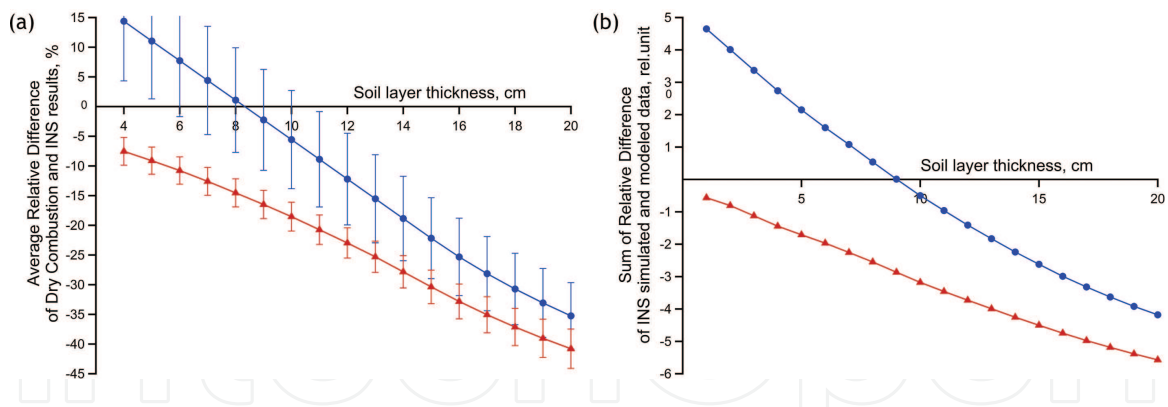


Figure 28. The dependence of average values of relative differences for weight percent (circles) and for surface densities (triangles) for measurements (a) and for MC simulations (b) with h [79].

that the soil carbon content parameter (based on gamma spectra using uniform carbon-sand mixture calibration data) is the average carbon weight percent for a 10-cm soil layer.

Therefore, INS simulation results (value of $Cw\%_{INS,i,2}$) can be attributed to average carbon weight percent in the soil layer with thickness h . Since different carbon depth profiles (from constant levels to sharp declines) were used in the simulations, the parameter (average carbon weight percent in soil layer with thickness 10 cm) could be assigned to the value determined from any INS gamma spectra.

2.11.2. Average carbon weight percent measured by PFTNA and chemical analysis

Results of carbon content measurements (average weight percent in upper 10-cm soil layer and its standard deviation) are shown in **Table 4**. Measurements were conducted by two methods (dry combustion and PFTNA). For clarity, the data from the open field at the Camp Hill location are shown in **Figure 29**. These data demonstrate good agreement between methods, especially for average values over whole plots. It should be noted that the accuracy of the carbon concentration measurement using PFTNA is comparable to measured values when the carbon concentration value is ~ 1 w% or less. To increase the accuracy of INS measurement at low soil carbon levels, further modification of our system is required. Such modifications would include (i) optimizing the detector's positioning relative to the neutron generator; (ii) increasing the number of detectors; and (iii) optimizing radiation shielding.

Data on soil carbon content can be used in mapping. Two maps of carbon distribution in the upper soil layer on one of the surveyed fields based on neutron-gamma analysis (PFTNA methods, **Figure 30a**) and chemical analysis (dry combustion, **Figure 30b**) are shown for comparison. As can be seen, both of these maps are very similar to each other. It should be noted that it took more than 1.5 months to collect the data for carbon content mapping in **Figure 30b** (dry combustion method), while only 2 working days were required for collecting carbon content data mapped in **Figure 30a** (PFTNA methods).

2.12. Effect of soil density and moisture on gamma response intensity

Soil density and moisture are parameters which could impact soil carbon measurement results when using PFTNA. While increasing soil density should increase the macroscopic

Location	Site # or Plot #	MINS measurements			Dry combustion measurements		
		Carbon, w%	STD, w%	Plot average \pm STD, w%	Carbon, w%	STD, w%	Plot average \pm STD, w%
Camp Hill Open Field	OF1	2.20	0.29	2.23 \pm 0.45	2.85	0.25	2.25 \pm 0.51
	OF2	2.51	0.29		2.54	0.31	
	OF3	1.76	0.22		1.91	0.13	
	OF4	1.88	0.23		2.99	0.94	
	OF5	2.82	0.25		3.03	0.37	
	OF6	2.15	0.21		1.99	0.26	
	OF7	2.77	0.32		1.92	0.41	
	OF8	2.52	0.25		2.44	0.15	
	OF9	2.06	0.26		1.79	0.27	
	OF10	2.17	0.27		2.25	0.45	
	OF11	2.39	0.22		2.23	0.30	
	OF12	3.11	0.31		2.91	0.47	
	OF13	1.44	0.25		1.49	0.42	
	OF14	1.93	0.29		1.80	0.19	
	OF15	1.86	0.27		1.67	0.25	
Camp Hill Applied Field 2	AF2-1	1.22	0.38	1.59 \pm 0.45	2.00	0.34	1.48 \pm 0.46
	AF2-2	2.09	0.37		1.14	0.34	
	AF2-3	1.46	0.37		1.31	0.08	
Camp Hill Applied Field 3	AF3-1	1.44	0.43	1.77 \pm 0.37	1.96	0.34	1.90 \pm 0.53
	AF3-2	1.68	0.37		1.34	0.34	
	AF3-3	2.17	0.39		2.4	0.8	
Camp Hill Applied Field 4	AF4-1	2.59	0.42	2.33 \pm 0.34	1.58	0.34	2.12 \pm 0.46
	AF4-2	2.47	0.37		2.35	0.34	
	AF4-3	1.94	0.45		2.42	0.14	
E.V.Smith* Plots	S220	-	-	0.93 \pm 0.61	-	-	0.93 \pm 0.18
	S320	-	-	0.92 \pm 0.61	-	-	1.40 \pm 0.05
	S104	-	-	0.34 \pm 0.68	-	-	1.06 \pm 0.09
	S114	-	-	0.81 \pm 0.62	-	-	1.41 \pm 0.53
	S102	-	-	0.93 \pm 0.62	-	-	1.04 \pm 0.11
	S112	-	-	1.49 \pm 0.68	-	-	1.51 \pm 0.55

*The measurement was made for one site on these plots.

Table 4. Average carbon weight percent in the upper soil layer by dry combustion and PFTNA methods [79].

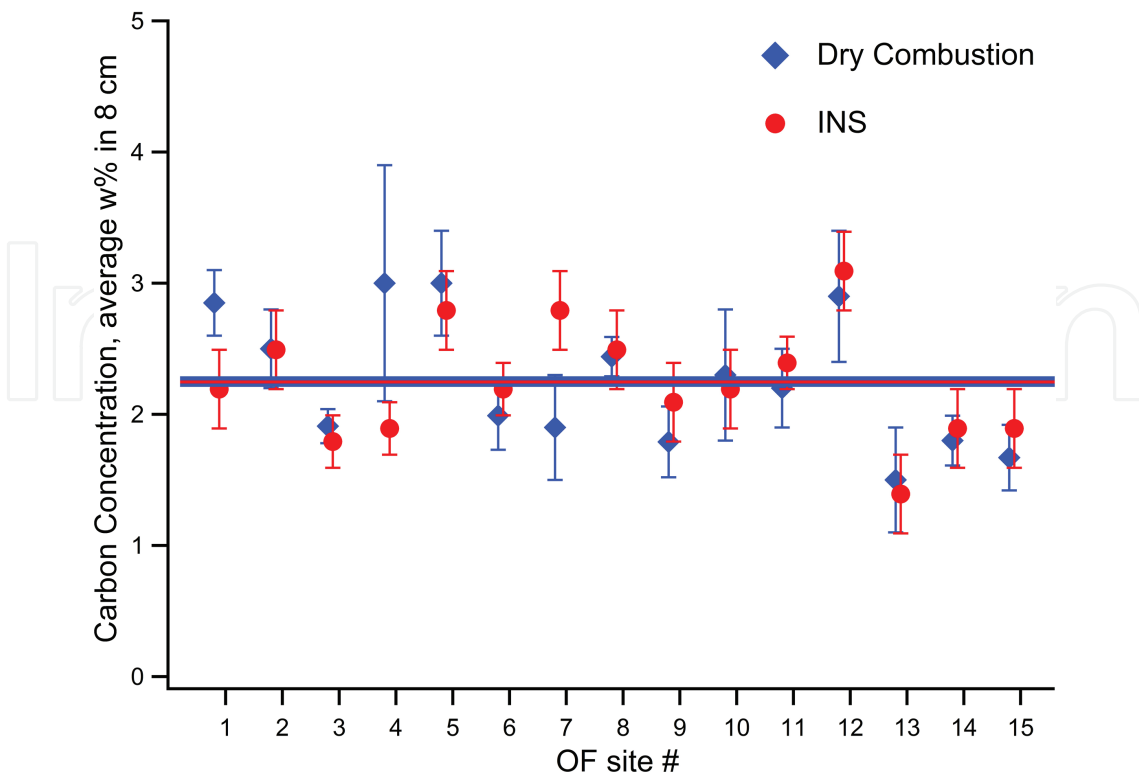


Figure 29. Average values of carbon weight percent for 10-cm soil layer measured by dry combustion (diamonds) and PFTNA (circles) methods for the open field (OF) site at Camp Hill (points) and average field values (solid lines) [79].

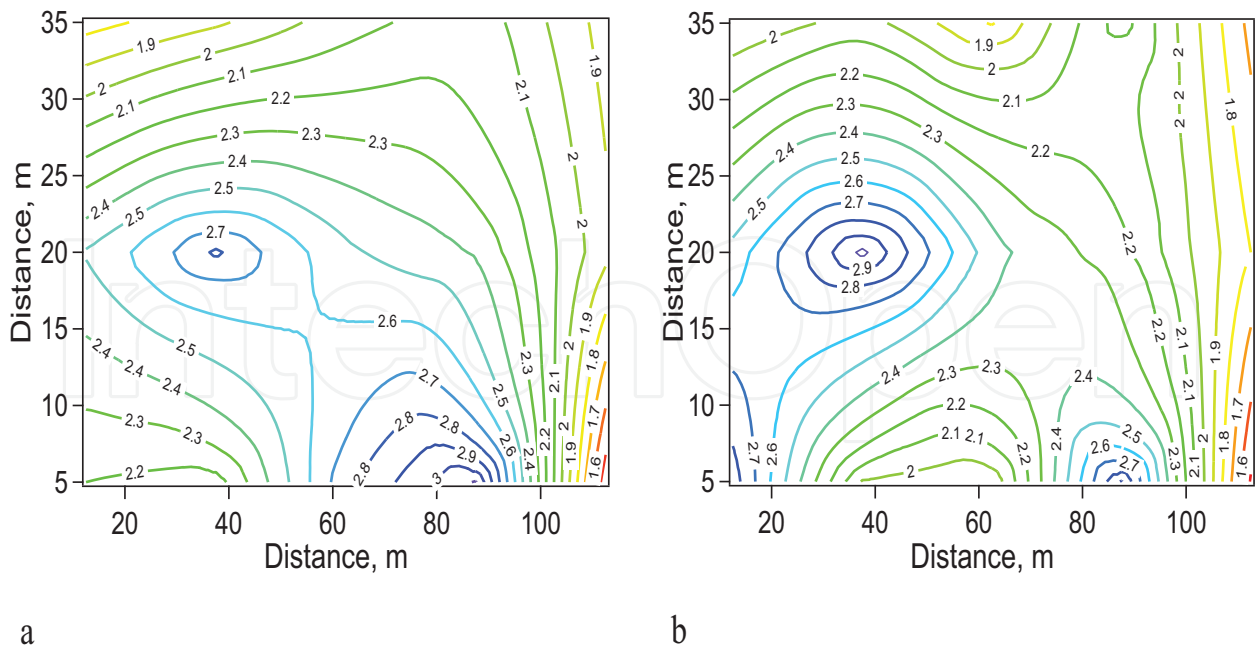


Figure 30. Carbon content maps of the upper layer of the open field (Piedmont Research Unit, Camp Hill, AL): (a) neutron-gamma analysis (PFTNA method) and (b) chemical analysis (dry combustion).

cross section of neutron interactions with soil nuclei, the excited soil volume could decrease. Thus, at first glance the effect of soil density on the peak of interest areas in the soil net INS spectra is not significant. The presence of soil moisture increases the amount of hydrogen atoms that run to faster neutron moderation and can decrease the peak of interest areas in the soil net INS spectra due to a decrease in fast neutron numbers. Using the Geant4 tool kit [82], MC simulations of gamma spectra for carbon-sand mixtures with different densities and moistures were conducted to estimate their effect on gamma response intensity. Both the INS and TNC spectra were simulated; the TNC processes were inactivated at INS spectra simulation (commands: /process/activate neutronInelastic, /process/inactivate nCapture, neutron data library JENDL4.0), while the INS processes were inactivated at TNC spectra simulation (commands: /process/activate nCapture, /process/inactivate neutronInelastic, neutron data library G4NDL4.5).

The simulated INS and TNC spectra for $150 \text{ cm} \times 150 \text{ cm} \times 60 \text{ cm}$ pits with 5w% carbon-sand mixtures of different densities (from 1.1 to 1.52 g/cm^3) are shown in **Figure 31**. The dependencies of peak of interest areas with centroids at 1.78 and 4.45 MeV in the INS spectra with densities are shown in **Figure 32**. As can be seen in these figures, there are no significant changes in the spectra or peak areas. Thus, there is no significant effect of soil density on the INS spectra.

Simulated INS and TNC spectra for $150 \text{ cm} \times 150 \text{ cm} \times 60 \text{ cm}$ pits with 5w% carbon-sand mixtures having different moistures H (H from 0 to 30% ; a real range of soil moisture change) are shown in **Figure 33**. The dependencies of peak of interest areas with centroids at 1.78 and 4.45 MeV in the INS spectra with water weight percent W [$W=H / (1+H)$] are shown in **Figure 34**. As seen in these figures, the peak areas slightly decrease throughout

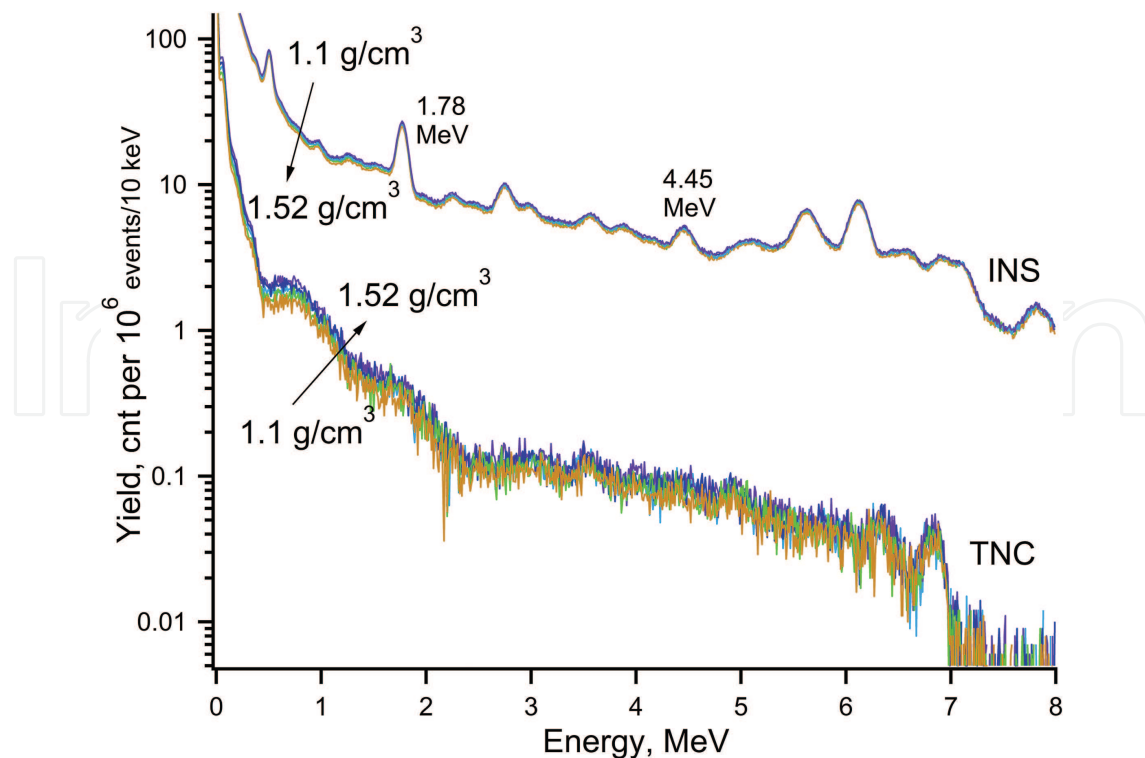


Figure 31. Geant4 simulated INS (JENDL4.0, $1e9$ events) and TNC (G4NDL4.5, $1e9$ events) gamma spectra for $150 \text{ cm} \times 150 \text{ cm} \times 60 \text{ cm}$ pits with 5w% carbon-sand mixtures with different densities (from 1.1 to 1.52 g/cm^3) irradiated by 14.1 MeV neutrons.

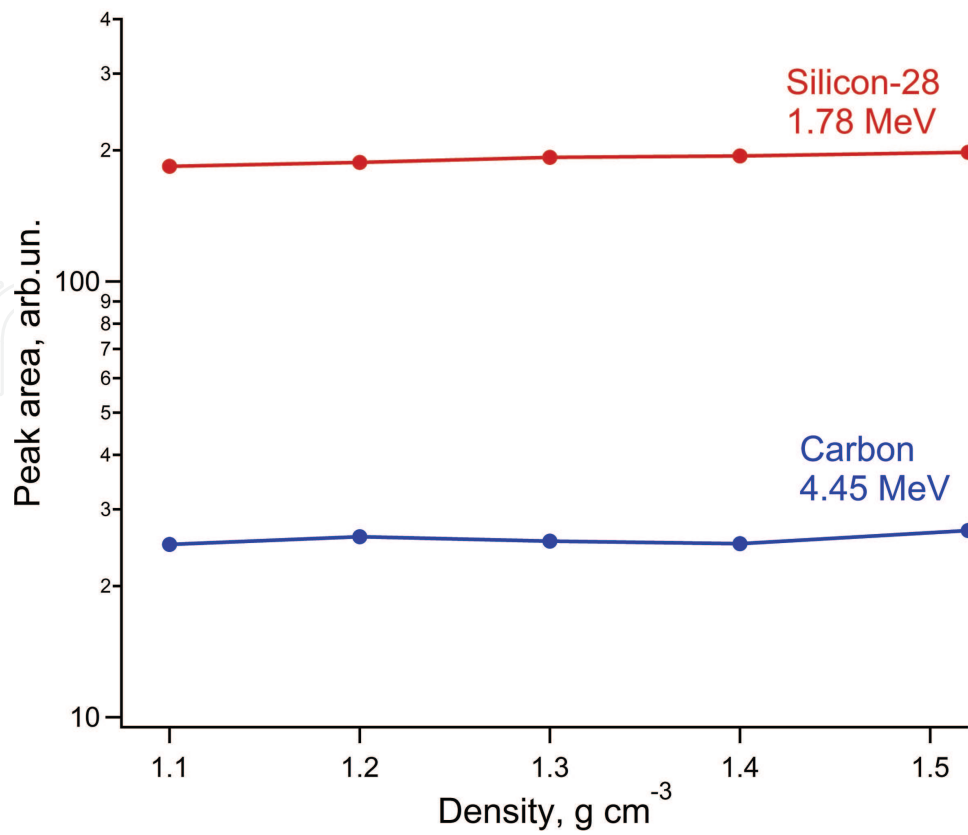


Figure 32. Dependencies of peak areas with centroids at 1.78 and 4.45 MeV with different densities in INS spectra shown in Figure 31.

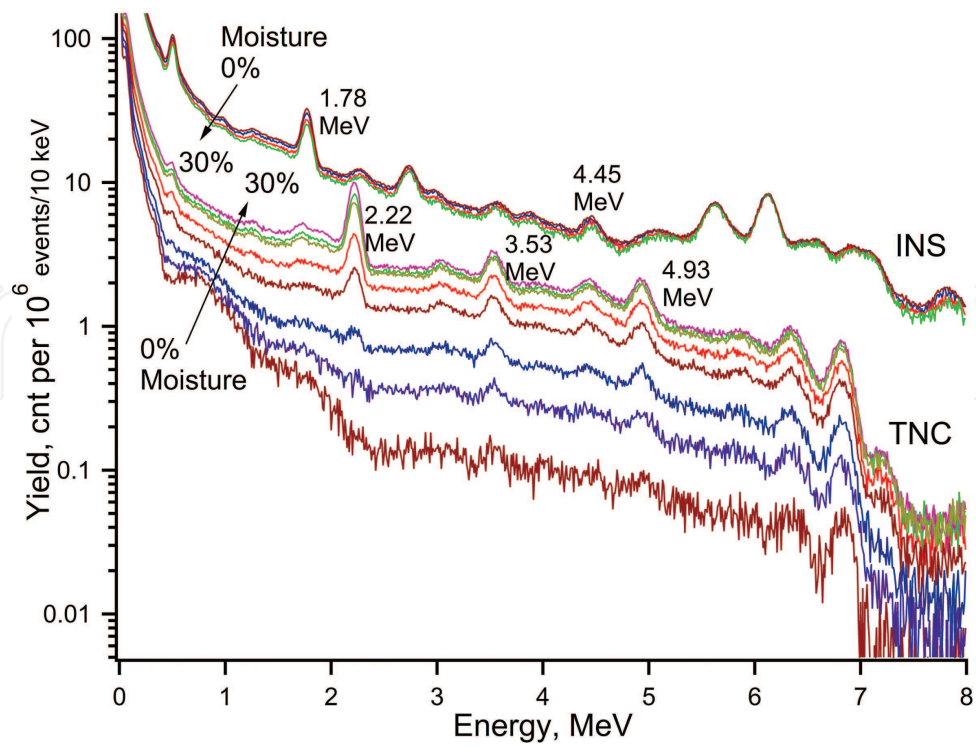


Figure 33. Geant4 simulated INS (JENDL4.0, 1e9 events) and TNC (G4NDL4.5, 1e9 events) gamma spectra for 150 cm × 150 cm × 60 cm pits with 5w% carbon-sand mixtures with different moistures (from 0 to 30%) irradiated by 14.1 MeV neutrons.

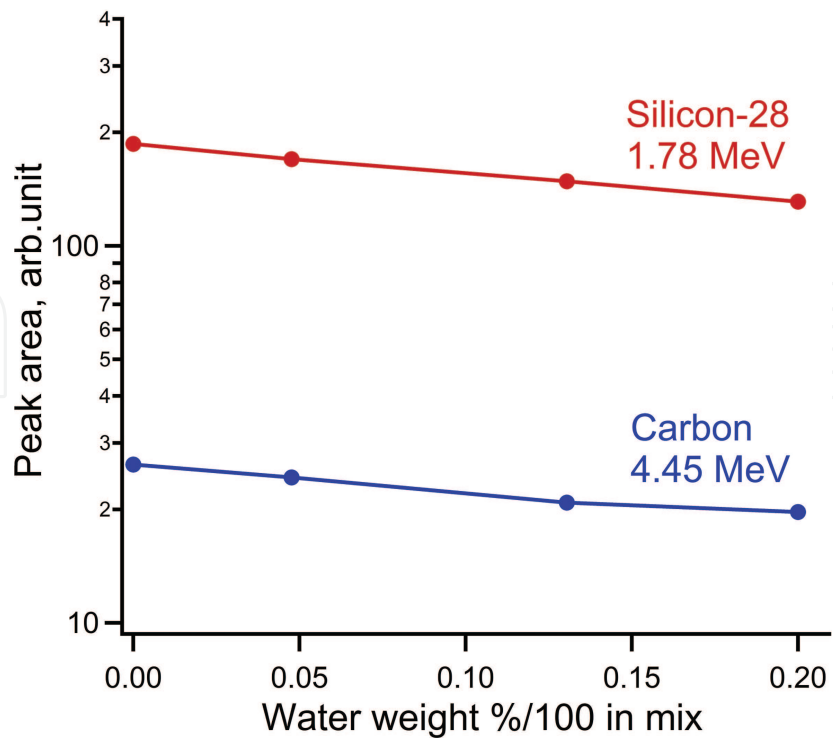


Figure 34. Dependencies of peak areas with centroids at 1.78 and 4.45 MeV with water weight percent in the INS spectra shown in Figure 33.

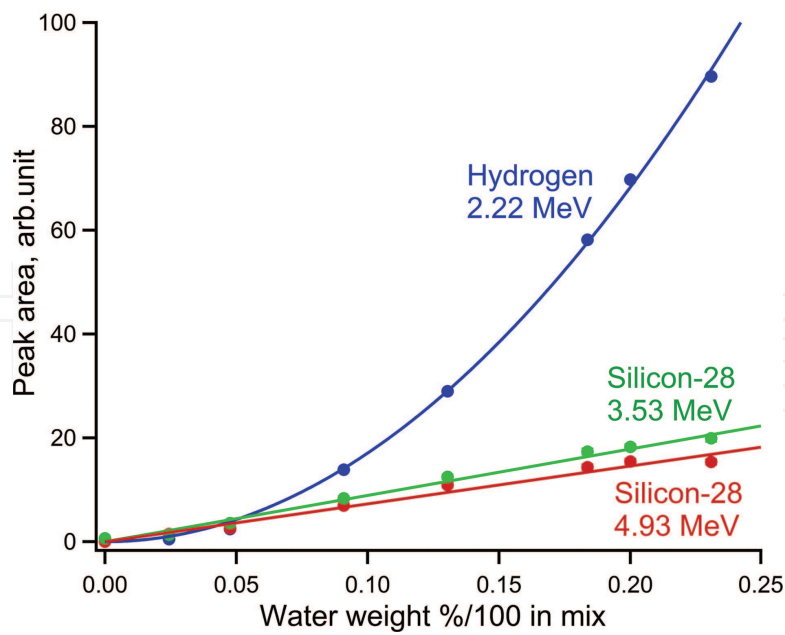


Figure 35. Dependencies of peak areas with centroids at 2.22, 3.53, and 4.93 MeV with water weight percent in the TNC spectra shown in Figure 33.

the possible moisture range. However, these changes are not significant in the practical range of soil moisture. Thus, it was concluded that moisture has no significant effect on the INS spectra.

At the same time, TNC spectra of gamma response increase with increasing soil moisture. In the studied moisture range, some peaks increase in direct proportion to the water weight percent in soil (e.g., TNC Si peaks with centroids at 3.53 and 4.93 MeV). The hydrogen peak with a centroid at 2.22 MeV increases as a square of the water weight percent within error limits (**Figure 35**). This probably occurs due to the linear increase of both thermal neutron flux and number of hydrogen nuclei as water weight percent increases. The conclusions regarding moisture and density effects on soil INS gamma response spectra agree with findings of others [15, 87].

3. Conclusion

Results of the PFTNA and the “gold standard” chemical analysis (Dry Combustion Technique) demonstrated good agreement for soil carbon content measurements in the upper soil layer (~10 cm). Experimental results successfully demonstrated that the average carbon weight percent in the upper soil layer (regardless of carbon depth distribution shape) can be measured *in situ* by the PFTNA measurement method (1 h) with accuracy comparable to the “gold standard” technique. The described procedures for background accountability, system calibration, and “soil carbon net peak” area calculations from the acquired spectra should be utilized. Although the current mobile system for PFTNA is fully capable of routine soil carbon measurements in natural and agricultural field settings, future modifications of the detector system and shielding can improve measurement accuracy and decrease measurement time. Nevertheless, the main features and herein described procedures (i.e., system background determination, calibration procedure, and “soil carbon net peak” area extraction) indicate that PFTNA methods can be recommended as a viable alternative procedure for soil carbon measurement. Additionally, MC simulations showed that soil density and moisture do not significantly impact soil carbon measurements by PFTNA.

Acknowledgements

The authors are indebted to Barry G. Dorman, Robert A. Icenogle, Juan Rodriguez, Morris G. Welch, and Marlin Siegford for technical assistance in experimental measurements, and to Jim Clark and Dexter LaGrand for assistance with computer simulations. We thank XIA LLC for allowing the use of their electronics and detectors in this project. This work was supported by NIFA ALA Research Contract No ALA061-4-15014 “Precision geospatial mapping of soil carbon content for agricultural productivity and lifecycle management.”

Author details

Aleksandr Kavetskiy, Galina Yakubova, Stephen A. Prior and Henry Allen Torbert*

*Address all correspondence to: allen.torbert@ars.usda.gov

USDA-ARS National Soil Dynamics Laboratory, Auburn, Alabama, USA

References

- [1] Valkovic V. 14 MeV Neutrons: Physics and Applications. CRC Press: Taylor & Francis Group; 2016, 481 p. DOI:10.1063/1.3120103
- [2] Aleksahkin V, Bystritsky V, Zamyatin N, Zubarev E, Krasnoperov A, Rapatsky V, Rogov YU, Sadovsky A, Salamatin A, Salmin R, Sapozhnikov M, Slepnev V, Khabarov S, Razinkov E. Detection of diamonds in kimberlite by the tagged neutron method. *Nuclear Instruments and Methods in Physics Research A*. 2015; **785**:9–13. DOI:10.1016/j.nima.2015.02.049
- [3] Parsons A, Bodnarik J, Evans L, Floyd S, Lim L, McClanahan T, Namkung M, Nowicki S, Schweitzer J, Starr R, Trombka J. Active neutron and gamma-ray instrumentation for in situ planetary science applications. *Nuclear Instruments and Methods in Physics Research A*. 2011; **652**:674–679. DOI:10.1016/j.nima.2010.09.157
- [4] Miceli A, Festa G, Gorini G, Senesi R, Andreani C. Pulsed neutron gamma-ray logging in archaeological site survey. *Measurement Science and Technology*. 2013; **24**:125903–125908. DOI:10.1088/0957-0233/24/12/125903
- [5] Tykot R. Scientific methods and applications to archaeological provenance studies. In: *Physics Methods in Archaeometry. Proceedings of the International School of Physics “Enrico Fermi”*. Martini M, Milazzo M, Piacentini M, editors. Bologna, Italy: Società Italiana di Fisica; 2014, pp. 407–432.
- [6] Panjeh H, Izadi-Najafabadi R. Body composition analyzer based on PGNA method. In: *Radioisotopes—Applications in Physical Sciences*. Nirmal S, editor. InTech; 2011, pp. 311–324. ISBN 978-953-307-510-5.
- [7] Chichester D, Empey E. Measurement of nitrogen in the body using a commercial PGNA system—phantom experiments. *Applied Radiation and Isotopes*. 2004; **60**:55–61. DOI:10.1016/j.apradiso.2003.09.007
- [8] Mitra S, Wolff J, Garrett R, Peters C. Application of the associated particle technique for the whole-body measurement of protein, fat and water by 14 MeV neutron activation analysis—a feasibility study. *Physics in Medicine and Biology*. 1995; **40**:1045–1055.

- [9] Mitra S, Wolff J, Garrett R. Calibration of a prototype *in vivo* total body composition analyzer using 14 MeV neutron activation and the associated particle technique. *Applied Radiation and Isotopes*. 1998; **49**:537–539.
- [10] Thermo Fisher Scientific Inc. 2016. Available from: <http://www.thermofisher.com/search/browse/results?customGroup=Neutron+Generators> [Accessed: 2017-01-26]
- [11] Dep L, Belbot M, Vourvopoulos G, Sudar S. Pulsed neutron-based on-line coal analysis. *Journal Radioanalytical Nuclear Chemistry*. 1998; **234**:107–112. DOI:10.1007/BF02389756
- [12] Saleh H, Livingston R. Experimental evaluation of a portable neutron-based gamma-spectroscopy system for chloride measurements in reinforced concrete. *Journal of Radioanalytical and Nuclear Chemistry*. 2000; **244**:367–371. DOI:10.1023/A:1006787626016
- [13] Naqvi A, Kalakada Z, Al-Matouq F, Maslehuddin M. Prompt gamma-ray analysis of chlorine in superpozz cement concrete. *Nuclear Instruments and Methods in Physics Research A*. 2012; **693**:67–73. DOI:10.1016/j.nima.2012.06.059
- [14] Nikitin A, Bliven S. Needs of well logging industry in new nuclear detectors. *Nuclear Science Symposium Proceedings*. 2010; 1214–1219. DOI:10.1109/NSSMIC.2010.5873961
- [15] Wielopolski L. Nuclear methodology for non-destructive multi-elemental analysis of large volumes of soil. In: *Planet Earth: Global Warming Challenges and Opportunities for Policy and Practice*. Carayannis E, editor. 2011, pp. 467–492. DOI:10.5772/23230
- [16] Seybold C, Mausbach M, Karlen D, Rogers H. Quantification of soil quality. *Soil Processes and the Carbon Cycle*. In: Lal R, Kimble J, Stewart B, editors. Boca Raton; FL: CRC Press; 1997, pp. 387–404
- [17] Potter K, Daniel J, Altom W, Torbert H. Stocking rate effect on soil carbon and nitrogen in degraded soils. *Journal of Soil Water Conservation*. 2001; **56**:233–236
- [18] Torbert H, Prior S, Runion G. Impact of the return to cultivation on carbon (C) sequestration. *Journal of Soil Water Conservation*. 2004; **59**:1–8
- [19] Stolbovoy V, Montanarella L, Filippi N, Jones A, Gallego J, Grassi G. Soil sampling protocol to certify the changes of organic carbon stock in mineral soil of the European Union. Version 2. EUR 21576 EN/2. Luxembourg: Office for Official Publications of the European Communities; 2007, 56 pp. ISBN 978-92-79-05379-5
- [20] Smith K, Watts D, Way T, Torbert H, Prior S. Impact of tillage and fertilizer application method on gas emissions (CO₂, CH₄, N₂O) in a corn cropping system. *Pedosphere*. 2012; **22**:604–615
- [21] Gilmore G. *Practical Gamma-Ray Spectrometry*. 2nd ed. West Sussex, England: Wiley; 2008, 387 p
- [22] NNDC. Upton, NY: Brookhaven National Laboratory; 2013. Available at: <http://www.nndc.bnl.gov/chart> [Accessed: 2017-01-26]

- [23] Yang J, Yang Y, Li Y, Tuo X, Li Z, Cheng Y, Mou Y, Huang W. Prompt gamma neutron activation analysis for multi-element measurement with series samples. *Laser Physics Letters*. 2013; **10**:1–5. DOI:10.1088/1612-2011/10/5/056002
- [24] Mernagh J, Harrison J, McNeill K. *In vivo* determination of nitrogen using Pu-Be sources. *Physics in Medicine and Biology*. 1977; **22**:831–835.
- [25] Shue S, Faw R, Shultis J. Thermal-neutron intensities in soils irradiated by fast neutrons from point sources. *Chemical Geology*. 1998; **144**:47–61. DOI:10.1016/S0009-2541(97)00108-3
- [26] Chung C, Tseng T-C. *In situ* prompt gamma-ray activation analysis of water pollutants using a shallow ^{252}Cf -HPGe Probe. *Nuclear Instruments and Methods in Physics Research Section A*. 1988; **267**:223–230. DOI:10.1016/0168-9002(88)90651-1
- [27] Barzilov A, Novikov I, Womble P. Material analysis using characteristic gamma rays induced by neutrons, gamma radiation. In: *Gamma Radiation*. Adrovic F, editor. InTech; 2012. Available from: <http://www.intechopen.com/books/gamma-radiation/material-analysis-using-characteristic-gamma-rays-induced-by-pulse-neutrons>. DOI:10.5772/2054
- [28] NRC. 2010. Available from: <http://www.nrc.gov/docs/ML1122/ML11229A704.pdf> [Accessed: 2017-01-26]
- [29] Industrial Radiation Sources. Eckert & Ziegler. 2008. Available from: http://www.ezag.com/fileadmin/ezag/user-uploads/isotopes/isotopes/5_industrial_sources.pdf [Accessed: 2017-01-26]
- [30] HPS (Health Physics Society). 2015. Available from: <https://hps.org/publicinformation/ate/q8216.html> [Accessed: 2017-01-26]
- [31] FTC (Frontier Technology Corporation). 2015. Available from: <http://www.frontier-cf252.com/index.html> [Accessed: 2017-01-26]
- [32] Sodern. 2015. http://www.sodern.com/sites/en/ref/Neutron-generator_79.html [Accessed: 2017-01-26]
- [33] Thermo Fisher Scientific Inc. 2016. Available from: <https://www.thermofisher.com/order/catalog/product/19187> [Accessed: 2017-01-26]
- [34] VNIIA. 2015. Available from: <http://vniia.ru/eng/ng/element.html> [Accessed: 2017-01-26]
- [35] Saint-Gobain. Scintillation products. Technical Note. 2009. Available from: http://www.crystals.saint-gobain.com/sites/imdf.crystals.com/files/documents/brilliance_performance_summary.pdf [Accessed: 2017-01-26]
- [36] Feng X, Cheng C, Yin Z, Khamlary M, Townsend P. Two kinds of deep hole-traps in $\text{Bi}_4\text{Ge}_3\text{O}_{12}$ crystals. *Chinese Physics Letters*. 1992; **9**:597–600.
- [37] Naqvi A, Kalakada Z, Al-Matouq F, Maslehuddin M, Al-Amoudi O. Chlorine detection in fly ash concrete using a portable neutron generator. *Applied Radiation and Isotopes*. 2012; **70**:1671–1674.

- [38] Van Loef E, Dorenbos P, van Eijk C, Krämer K, Güdel H. High-energy-resolution scintillator: Ce^{3+} activated $LaBr_3$. *Applied Physics Letters*. 2001; **79**:1573–1575. DOI:10.1063/1.1385342
- [39] McFee J, Faust A, Andrews H, Kovaltchouk V, Clifford E, Ing H. A comparison of fast inorganic scintillators for thermal neutron analysis landmine detection. *IEEE Transactions on Nuclear Science*. 2009; **56**:1584–1592. DOI:10.1109/TNS.2009.2018558
- [40] Turner J. *Atom, Radiation and Radiation Protection*. 3rd ed. Weinheim, Germany: Wiley-VCH Verlag GmbH & Co. KGaA; 2007, 586 p. ISBN 978-3-527-40606-7
- [41] Kavetskiy A, Yakubova G, Torbert H, Prior S. Application of Geant4 simulation for analysis of soil carbon inelastic neutron scattering measurements. *Applied Radiation and Isotopes*. 2016; **113**:33–39. DOI:10.1016/j.apradiso.2016.04.013
- [42] Sudac D, Valkovic V. Irradiation of 4"×4" NaI(Tl) detector by the 14 MeV neutrons. *Applied Radiation and Isotopes*. 2010; **68**:896–900. DOI:10.1016/j.apradiso.2009.12.014
- [43] IAEA. Neutron generators for analytical purposes. 2012, 162 p. ISSN 2225-8833(1). Available from: http://www-pub.iaea.org/MTCD/Publications/PDF/P1535_web.pdf [Accessed: 2017-01-26]
- [44] Saint-Gobain. Efficiency calculations for selected scintillators. Available from: <http://www.crystals.saint-gobain.com/uploadedFiles/SG-Crystals/Documents/Technical/SGC%20Efficiency%20Calculations%20Brochure.pdf> [Accessed: 2017-01-26]
- [45] Naqvi A, Maslehuddin M, Kalakada Z, Al-Amoudi O. Prompt gamma ray evaluation for chlorine analysis in blended cement concrete. *Applied Radiation and Isotopes*. 2014; **94**:8–13. DOI:10.1016/j.apradiso.2014.06.011
- [46] Womble P, Vourvopoulos G, Paschal J, Novikov I, Barzilov A. Results of field trials for the PELAN system. *Proceedings of SPIE*. 2002; **4786**: 52–57. DOI:10.1117/12.450506
- [47] Bystritsky V, Zubarev E, Krasnoperov A, Porohovoi S, Rapatskii V, Rogov Yu, Sadovskii A, Salamatin A, Salmin R, Slepnev V, Andreev E. Gamma detectors in explosives and narcotics detection systems. *Physics of Particles and Nuclei Letters*. 2013; **10**: 566–572. DOI:10.1134/S154747711306006X
- [48] Ozdemir T, Akbay I, Uzun H, Reyhancan I. Neutron shielding of EPDM rubber with boric acid: mechanical, thermal properties and neutron absorption tests. *Progress in Nuclear Energy*. 2016; **89**:102–109. DOI:10.1016/j.pnucene.2016.02.007
- [49] Elmahroug Y, Tellili B, Souga C. Calculation of gamma and neutron shielding parameters for some materials polyethylene-based. *International Journal of Physics and Research*. 2013; **3**:33–40
- [50] Singh V, Badiger N. Investigation of gamma and neutron shielding parameters for borate glasses containing NiO and PbO. *Physics Research International*. 2014. Available from: <https://www.hindawi.com/journals/physri/2014/954958/> [Accessed: 2017-01-26]. DOI:10.1155/2014/954958

- [51] Elsheikh N, Habbani F, ElAgib I. Investigations of shield effect and type of soil on landmine detection. *Nuclear Instruments and Methods in Physics Research A*. 2011; **652**:1–4. DOI:10.1016/j.nima.2010.09.183
- [52] El-Bakkoush F, Akki T. Attenuation of neutrons and total gamma rays in two layers shields. *Journal of Nuclear Science and Technology*. 2000; **37**:526–529. DOI:10.1080/00223131.2000.10874943
- [53] Wielopolski L, Mitra S, Doron O. Non-carbon-based compact shadow shielding for 14 MeV neutrons. *Journal of Radioanalysis Nuclear Chemistry*. 2008; **276**:179–182. DOI:10.1007/s10967-007-0429-1
- [54] Bystritsky V, Valkovich V, Grozdanov D, Zontikov A, Ivanov I, Kopach Yu, Krulov A, Rogov Yu, Ruskov I, Sapoznikov M, Skoii V, Shvezov V. Multilayer passive shielding of the scintillation detectors on the base of BGO, NaI(Tl) and stilbene working in the intensive neutron fields with energy 14.1 MeV. *Physics of Particles and Nuclei Letters*. 2015; **12**:325–335. DOI:10.1134/S1547477115020089
- [55] Mitra S, Dioszedi I. Development of an instrument for non-destructive identification of unexploded ordnance using tagged neutrons—a proof of concept study. *IEEE Nuclear Science Symposium Conference Record*. 2011; 285–289. DOI:10.1109/NSSMIC.2011.6154499
- [56] Yakubova G, Wielopolski L, Kavetskiy A, Torbert H, Prior S. Field testing a mobile inelastic neutron scattering system to measure soil carbon. *Soil Science*. 2014; **179**:529–535. DOI:10.1097/SS.0000000000000099
- [57] Womble P, Schultz F, Vourvopoulos G. Non-destructive characterization using pulsed fast-thermal neutrons. *Nuclear Instrument and Methods in Physics Research Section B*. 1995; **99**:757–760. DOI:10.1016/0168-583X(95)00326-6
- [58] Nellis W. Slowing-down distances and times of 0.1–14 MeV neutrons in hydrogenous materials. *American Journal of Physics*. 1977; **45**:443–446. DOI:10.1119/1.10833
- [59] Miller V. Measuring the mean lifetime of thermal neutrons from a small specimen. *Atomnaya Energiya*. 1967; **22**:33–38. DOI:10.1007/BF01225391
- [60] Vourvopoulos G, Womble P. Pulsed fast/thermal neutron analysis: a technique for explosives detection. *Talanta*. 2001; **54**:459–468. DOI:10.1016/S0039-9140(00)00544-0
- [61] Mitra S, Wielopolski L. Optimizing the gate-pulse width for fast neutron induced gamma-ray spectroscopy. *Proceedings of SPIE*. 2005; **5923**(8):16. DOI:10.1117/12.614569
- [62] Nelson D, Sommers L. Total carbon, organic carbon, and organic matter. In: Sparks D, editor. *Methods of Soil Analysis*. Madison, WI: SSSA and ASA; 1996, pp. 961–1010.
- [63] Hendricks J. A Monte Carlo code for particle transport. *Los Alamos Science*. 1994; **22**:42–33.
- [64] Lux L, Koblinger L. *Monte Carlo particle transport methods: neutron and photon calculations*. Florida: CRC Press; 1991, 517 p

- [65] Deiev O. Geant4 simulation of neutron transport and scattering in media. *Problems of atomic science and technology. Series: Nuclear Physics Investigation*. 2013; **3**:236–241
- [66] Bak S, Park T-S, Hong S. Geant4 simulation of the shielding of neutrons from ^{252}Cf source. *Journal of the Korean Physical Society*. 2011; **59**:2071–2074. DOI:10.3938/jkps.59.2071
- [67] Reda A. Monte Carlo simulations of a D-T neutron generator shielding for landmine detection. *Radiation Measurements*. 2011; **46**:1187–1193. DOI:10.1016/j.radmeas.2011.07.013
- [68] Feng Z, Jun-tao L. Monte Carlo simulation of PGNA system for determining element content in the rock sample. *Journal of Radioanalytical and Nuclear Chemistry*. 2014; **299**:1219–1224. DOI:10.1007/s10967-013-2858-3
- [69] Qin X, Zhou R, Han J-F, Yang C-W. GEANT4 simulation of the characteristic gamma-ray spectrum of TNT under soil induced by DT neutrons. *Nuclear Science and Techniques*. 2015; **26**:010501-1–010501–6. DOI:10.13538/j.1001-8042/nst.26.010501
- [70] Nasrabadi M, Bakhshi F, Jalali M, Mohammadi A. Development of a technique using MCNPX code for determination of nitrogen content of explosive materials using prompt gamma neutron activation analysis method. *Nuclear Instruments and Methods in Physics Research Section A*. 2011; **659**:378–382. DOI:10.1016/j.nima.2011.08.029
- [71] Perot B, El Kanawati W, Carasco C, Eleon C, Valkovic V, Sudac D, Obhodas J, Sannie, G. Quantitative comparison between experimental and simulated gamma-ray spectra induced by 14 MeV tagged neutrons. *Applied Radiation and Isotopes*. 2012; **70**:1186–1192. DOI:10.1016/j.apradiso.2011.07.005
- [72] El Kanawati W, Perot B, Carasco C, Eleon C, Valkovic V, Sudac D, Obhodas J, Sannie G. Acquisition of prompt gamma-ray spectra induced by 14 MeV neutrons and comparison with Monte Carlo simulations. *Applied Radiation and Isotopes*. 2011; **69**:732–743. DOI:10.1016/j.apradiso.2011.01.010
- [73] Tain J, Agramunt J, Algora A, Aprahamian A, Cano-Ott D, Fraile L, Guerrero C, Jordan M, Mach H, Martinez T, Mendoza, Mosconi M, Nolte R. The sensitivity of $\text{LaBr}_3\text{:Ce}$ scintillation detectors to low energy neutrons: measurement and Monte Carlo simulation. *Nuclear Instruments and Methods in Physics Research Section A*. 2015; **774**:17–24. DOI:10.1016/j.nima.2014.11.060
- [74] Wielopolski L, Song Z, Orion I, Hanson A, Hendrey G. Basic considerations for Monte Carlo calculations in soil. *Applied Radiation and Isotopes*. 2005; **62**:97–107. DOI:10.1016/j.apradiso.2004.06.003
- [75] Doron O, Wielopolski L, Mitra S, Biegalski S. MCNP benchmarking of an inelastic neutron scattering system for soil carbon analysis. *Nuclear Instruments and Methods in Physics Research Section A*. 2014; **735**:431–436. DOI:10.1016/j.nima.2013.09.049

- [76] Wielopolski L, Yanai R, Levine C, Mitra S, Vadeboncoeur M. Rapid, non-destructive carbon analysis of forest soils using neutron-induced gamma-ray spectroscopy. *Forest Ecology Management*. 2010; **260**:1132–1137. DOI:10.1016/j.foreco.2010.06.039
- [77] Mitra S, Wielopolski L, Tan H, Fallu-Labruyere A, Hennig W, Warburton W. Concurrent measurement of individual gamma-ray spectra during and between fast neutron pulses. *Nuclear Science*. 2007; **54**:192–196. DOI:10.1109/TNS.2006.889165
- [78] Tan H, Mitra S, Wielopolski L, Fallu-Labruyere A, Hennig W, Chu Y, Warburton W. A multiple time-gated system for pulsed digital gamma-ray spectroscopy. *Journal of Radioanalysis Nuclear Chemistry*. 2008; **276**:639–643. DOI:10.1007/s10967-008-0611-0
- [79] Yakubova G, Kavetskiy A, Prior S, Torbert H. Benchmarking the inelastic neutron scattering soil carbon method. *Vadose Zone Journal*. 2016; **15**:1–11. DOI:10.2136/vzj2015.04.0056.
- [80] Murphy R, Kozlovsky B, Share G. Nuclear cross sections for gamma-ray de-excitation line production by secondary neutrons in the Earth's atmosphere. *Journal of Geophysics Research*. 2011; **116**:1–9. DOI:10.1029/2010JA015820
- [81] Herman M, Capote R, Carlson B, Oblozinsky P, Sin M, Trkov A, Wienke H, Zerkin V. EMPIRE: nuclear reaction model code system for data evaluation. *Nuclear Data Sheets*. 2007; **108**:2655–2715. DOI:10.1016/j.nds.2007.11.003
- [82] Agostinelli S, et al. GEANT4—a simulation toolkit. *Nuclear Instruments and Methods in Physics Research Section A: Accelerators, Spectrometers, Detectors and Associated Equipment*. 2003; **506**:250–303. DOI:10.1016/S0168-9002(03)01368-8
- [83] CERN, 2014. Geant4. Available from: <http://geant4.web.cern.ch/geant4/support/download.shtml> [Accessed: 2017-01-26]
- [84] Knoll G. *Radiation Detection and Measurement*. 3rd ed. New York: Wiley; 2000
- [85] WaveMetrics. 2013. IGORPro. Available from: <http://www.wavemetrics.com/products/igorpro/igorpro.htm> [Accessed: 2017-01-26]
- [86] Kavetskiy A, Yakubova G, Torbert H, Prior S. Continuous versus pulse neutron induced gamma spectroscopy for soil carbon analysis. *Applied Radiation and Isotopes*. 2015; **96**:139–147. DOI:10.1016/j.apradiso.2014.10.024
- [87] Doron O. Simulation of an INS soil analysis system [thesis]. Austin: The University of Texas at Austin; 2007. Available from: <http://www.library.utexas.edu/etd/d/2007/dorono09518/dorono09518.pdf> [Accessed: 2017-01-26]